Journal of Experimental Botany
https://doi.org/10.1093/jxb/erac013 Advance Access Publication 19 January, 2022

RESEARCH PAPER

Polycomb proteins control floral determinacy by H3K27me3-mediated repression of pluripotency genes in *Arabidopsis thaliana*

Ralf Müller-Xing[1,2,3,4,*,†], Rhomi Ardiansyah[1,2,3,†], Qian Xing[1,2,3,4,*,†], Léa Faivre[5,†], Jingjing Tian[1,2,3,†], Guohua Wang[6,7], Yucai Zheng[1,2,3], Xue Wang[3], Tingting Jing[1,2,3], Erica de Leau[4], Song Chen[6], Su Chen[6], Daniel Schubert[5] and Justin Goodrich[4]

[1] Lushan Botanical Garden, Chinese Academy of Sciences, Jiujiang, China
[2] Key Laboratory of Saline-Alkali Vegetation Ecology Restoration (Northeast Forestry University), Ministry of Education, Harbin, China
[3] Plant Epigenetics and Development, Institute of Genetics, College of Life Science, Northeast Forestry University, Harbin, China
[4] Institute of Molecular Plant Sciences, The University of Edinburgh, Edinburgh, UK
[5] Epigenetics of Plants, Freie Universität Berlin, Berlin, Germany
[6] State Key Laboratory of Tree Genetics and Breeding, Northeast Forestry University, Harbin, China
[7] Information and Computer Engineering College, Northeast Forestry University, Harbin, China

[†] These authors contributed equally to this work.
* Correspondence: Ralf.Mueller@hhu.de or QXing@lsbg.cn

Received 22 June 2021; Editorial decision 13 January 2022; Accepted 17 January 2022

Editor: Joanna Putterill, University of Auckland, New Zealand

Abstract

Polycomb group (PcG) protein-mediated histone methylation (H3K27me3) controls the correct spatiotemporal expression of numerous developmental regulators in Arabidopsis. Epigenetic silencing of the stem cell factor gene *WUSCHEL* (*WUS*) in floral meristems (FMs) depends on H3K27me3 deposition by PcG proteins. However, the role of H3K27me3 in silencing of other meristematic regulator and pluripotency genes during FM determinacy has not yet been studied. To this end, we report the genome-wide dynamics of H3K27me3 levels during FM arrest and the consequences of strongly depleted PcG activity on early flower morphogenesis including enlarged and indeterminate FMs. Strong depletion of H3K27me3 levels results in misexpression of the FM identity gene *AGL24*, which partially causes floral reversion leading to *ap1*-like flowers and indeterminate FMs ectopically expressing *WUS* and *SHOOT MERISTEMLESS* (*STM*). Loss of *STM* can rescue supernumerary floral organs and FM indeterminacy in H3K27me3-deficient flowers, indicating that the hyperactivity of the FMs is at least partially a result of ectopic *STM* expression. Nonetheless, *WUS* remained essential for the FM activity. Our results demonstrate that PcG proteins promote FM determinacy at multiple levels of the floral gene regulatory network, silencing initially floral regulators such as *AGL24* that promotes FM indeterminacy and, subsequently, meristematic pluripotency genes such as *WUS* and *STM* during FM arrest.

Keywords: Epigenetic gene regulation, floral organ specification, floral stem cell determinacy, flower development, MADS box genes, PcG proteins.

Introduction

In plants, the epigenetic machinery provides stable gene expression patterns, which enable the formation of various tissues and whole organs including roots, shoots, and flowers (Xiao *et al.*, 2017; Jing *et al.*, 2020). All aerial parts of plants are formed from the shoot apical meristem (SAM) (Nägeli, 1858) carrying a self-maintaining stem cell pool that enables lifelong organogenesis (Williams and Fletcher, 2005; Soyars *et al.*, 2016). The homeostasis of this stem cell niche depends on a negative feedback loop in *Arabidopsis thaliana* (Arabidopsis): the transcription factor (TF) WUSCHEL (WUS) is expressed in cells of the organizing center (OC) directly underneath the stem cells. Intercellular movement of WUS from the OC to the stem cells at the top of the SAM is required for non-cell-autonomous maintenance of the stem cells and activates the stem cell-specific *CLAVATA 3* (*CLV3*) gene encoding a small secreted signal peptide (Fletcher *et al.*, 1999; Schoof *et al.*, 2000; Yadav *et al.*, 2011; Daum *et al.*, 2014). In turn, the CLV3 peptide is perceived by receptor kinases including CLAVATA 1 (CLV1) and CLV2-CORYNE (CRN) in the underlying cells of the OC to dampen *WUS* expression (Brand *et al.*, 2000; Müller *et al.*, 2006, 2008). In this feedback loop, WUS promotes stem cell fate and *CLV3* expression, while CLV3 represses *WUS*. This feedback regulation maintains the size of the OC and stem cell niche and, ultimately, the size and function of the SAM (Somssich *et al.*, 2016). Furthermore, several members of the homeodomain (HD) TF superfamily play a vital role in determining meristem functions including the BEL1-like (BELL) members PENNYWISE (PNY) and POUNDFOOLISH (PNF) and the four members of the KNOX/KNAT (for KNOTTED-like from *Arabidopsis thaliana*) class I, SHOOT MERISTEMLESS (STM), BREVIPEDICELLUS (BP)/KNAT1, KNAT2, and KNAT6 (Scofield and Murray, 2006). Recently, it was shown that WUS–STM protein interaction enhances the binding of WUS to the *CLV3* promoter, which in turn is required to regulate *CLV3* expression and to maintain a constant number of stem cells (Su *et al.*, 2020).

After transition from the vegetative to the reproductive phase, the SAM converts into an inflorescence meristem (IM) producing flowers at its flanks. The floral meristems (FMs) generate primordia of the flower organs which are organized in four whorls: four sepals in whorl 1, four petals in whorl 2, six stamens in whorl 3, and two fused carpels in whorl 4 (Alvarez-Buylla *et al.*, 2010). Antagonistic interaction between the IM identity genes, *TERMINAL FLOWER 1* (*TFL1*) and *AGAMOUS-LIKE 24* (*AGL24*), and the FM identity genes, *LEAFY* (*LFY*), *APETALA 1* (*AP1*), and *CAULIFLOWER* (*CAL*), maintains the identity of both types of SAMs (Bradley *et al.*, 1997; Liljegren *et al.*, 1999; Ratcliffe *et al.*, 1999). *AP1* and *CAL* encode MADS domain TFs that have partially redundant activities involved in the formation of FMs by repression of *TFL1* (Ratcliffe *et al.*, 1999; Kempin *et al.*, 1995). In turn, *TFL1* bars *AP1* and *LFY* expression in IMs (Liljegren *et al.*, 1999; Ratcliffe *et al.*, 1999). *LFY* encodes a plant-specific TF that activates *AP1* but also *TFL1* expression, suggesting that *LFY* and *AP1/CAL* have partially antagonistic activities in the control of floral initiation (Goslin *et al.*, 2017; Serrano-Mislata *et al.*, 2017).

The ABC model describes how a few genes act together to specify the four types of flower organs (Coen and Meyerowitz, 1991; Causier *et al.*, 2010): sepals are specified by A-function genes, petals by a combination of A- and B-function genes, stamens by B- and C-function genes, and C-function alone specifies carpels. LFY activates the expression of the ABC-type MADS domain TFs AP1 (class A), APETALA 3 and PISTILLATA (AP3 and PI; both class B), and AGAMOUS (AG; class C) that also terminates *WUS* expression in FMs (Causier *et al.*, 2010). The molecular basis of floral organ identity specification is the combinatorial formation of tetrameric complexes between the ABC-type MADS domain TFs with the E function MADS domain TFs, SEPALLATA 1–4 (SEP1–SEP4) (Pelaz *et al.*, 2000; Ditta *et al.*, 2004; Melzer *et al.*, 2009).

FM specification also requires the down-regulation of the MADS box and flowering time genes *FRUITFULL* (*FUL*), *SUPPRESSOR OF OVEREXPRESSION OF CONSTANS 1* (*SOC1*), *SHORT VEGETATIVE PHASE* (*SVP*), and *AGL24* by direct binding of AP1 (Yu *et al.*, 2004; Liu *et al.*, 2007; Alvarez-Buylla *et al.*, 2010; Chu *et al.*, 2010; Kaufmann *et al.*, 2010). Overexpression of *AGL24* causes FMs to revert to IMs, phenocopying *ap1* mutant flowers with secondary flowers in the axils of leaf-like sepals (Yu *et al.*, 2004; Liu *et al.*, 2007). During stage 1 and 2 of flower development, AGL24 and SVP form dimers with AP1 to repress directly the class B, C, and E floral homeotic genes *AP3*, *PI*, *AG*, and *SEP3* (Gregis et al., 2006, 2009; Liu *et al.*, 2009). *AGL24* and *SVP* are also FM identity genes since the *ap1 svp agl24* triple mutant continuously produces IMs in place of flowers (Gregis *et al.*, 2008). Furthermore, AGL24 acts redundantly with SOC1, SVP, and SEP4, directly suppressing *TFL1* in emerging FMs, which prevents floral reversion (Liu *et al.*, 2013). These findings indicate that *AGL24* has features of an IM as well as an FM identity gene.

All above-mentioned TFs are targets of the epigenetic repressive mark H3K27me3 (tri-methylation of Lys27 on histone H3), which is associated with Polycomb (PcG) function (Zhang *et al.*, 2007; Lafos *et al.*, 2011). The SET domain-containing histone methyltransferase (HMT) Enhancer of zeste [E(z)], which is the catalytic subunit of the Polycomb Repressive Complex 2 (PRC2), silences PcG target genes by H3K27me3 (Schuettengruber *et al.*, 2017). In Arabidopsis, E(z) is encoded by three homologs including *CURLY LEAF* (*CLF*) and *SWINGER* (*SWN*) (Spillane *et al.*, 2000; Mozgova and Hennig, 2015). One further core component of PRC2 is Suppressor of zeste 12 [Su(z)12], which is encoded by three homologs including *EMBRYONIC FLOWER 2* (*EMF2*) and

VERNALIZATION 2 (*VRN2*) in Arabidopsis (Chanvivattana *et al.*, 2004). Like *CLF* and *SWN*, *EMF2* and *VRN2* are essential for the post-embryonic development since severe *emf2-3 vrn2-1* and *clf swn* mutant seedlings form only callus-like tissue after germination (Schubert *et al.*, 2005). Recently, we introduced two plant lines with strongly depleted PcG activity, *clf-28 swn-7 CLF-GR* (*iCLF*) and *emf2-10 vrn2-1* double mutants, which form leaves and shoots bearing flowers with diverse defects, although global H3K27me3 levels are highly reduced (Lafos *et al.*, 2011; Müller-Xing et al., 2014, 2015).

Normal flower development requires both initiation and termination of the floral stem cell niche by the balance between the positive stem cell factor WUS and the negative regulator AG, which form a positive–negative feedback loop (Lenhard *et al.*, 2001; Lohmann *et al.*, 2001; Ming and Ma, 2009). After initiating in stage 2, WUS activates, together with LFY, the expression of *AG*. In turn, AG represses *WUS* expression that completely vanishes during floral stage 6, followed by loss of the floral stem cell pool (Lenhard *et al.*, 2001; Lohmann *et al.*, 2001). The silencing of *WUS* is accompanied by direct recruitment of PRC2 and, subsequently, H3K27me3 deposition at the *WUS* chromatin (Liu *et al.*, 2011; Sun *et al.*, 2019). Nevertheless, the significance of H3K27me3 deposition for gene silencing of other meristematic genes during termination of the floral stem cell population remained largely unclear.

In our study, we explored the impact of cumulative H3K27me3 levels on early flower morphogenesis using a combined approach of mutant analyses and genome-wide profiling of H3K27me3. Strongly depleted PcG activity results in enlarged and indeterminate FMs consistent with increased and prolonged stem cell activity. Surprisingly, we found evidence that this hyperactivity of the FMs is partially independent of *WUS* expression levels, giving rise to the possibility that PcG proteins control FM size and determinacy also through silencing of other meristematic regulators. We identified candidates by genome-wide H3K27me3 profiling during FM arrest and, subsequently, expression analysis in PcG mutants. Based on our double mutant and gene expression studies, we propose that the H3K27me3-mediated silencing of *AGL24* and *STM* is of similar importance as silencing of *WUS* for the control of FM determinacy by PcG proteins.

Materials and methods

Plant materials and growth conditions

Arabidopsis thaliana (L.) Heynh. plants were grown at 21 °C under long-day (16 h light/8 h dark) conditions, unless indicated otherwise. *iCLF* (*clf-28 swn-7 CLFpro::CLF-GR*, in Col-0 background), *emf2-10 vrn2-1* (Ws-0), and *emf2-10 vrn2-1* backcrossed to La-0 were described previously (Lafos *et al.*, 2011; Müller-Xing et al., 2014, 2015). *emf2-10 vrn2-1* (La-0) was backcrossed to L*er*-0 to generate *emf2-10 vrn2-1 erecta* (*ev er*) to obtain an Arabidopsis line with strongly depleted PcG activity in the *er* mutant background. In each experiment, the corresponding ecotype was used as the wild type control. *agl24-1* mutants (Michaels *et al.*, 2003) and *STM::GUS* (Kirch *et al.*, 2003) were kindly provided by R.M. Amasino and Wolfgang Werr, respectively. *clf-28 swn-7*, *clv1-11*, *clv3-2*, *crn-1*, *wus-1*, *WUS::GUS*, and *LEAFY::GUS* were previously described (Laux *et al.*, 1996; Blázquez *et al.*, 1997; Fletcher *et al.*, 1999; Gross-Hardt *et al.*, 2002; Diévart *et al.*, 2003; Schubert *et al.*, 2005; Müller *et al.*, 2008). *ap1-1* (Irish and Sussex, 1990) was obtained from the Nottingham Arabidopsis Stock Centre. The *35S::AP1-GR ap1-1 cal-1* line (Wellmer *et al.*, 2006) was kindly provided by Frank Wellmer and Yuling Jiao. After 3 weeks of short days (8 h light/16 h dark), the *35S::AP1-GR ap1-1 cal-1* plants were shifted to long days and, 5 d later, induced with dexamethasone. We crossed *clv1-11*, *crn-1*, *clv3-2*, *wus-1*, *ap1-1*, *agl24-1*, and *bum1-3* to *emf2-10 vrn2-1* and/or *iCLF*, to generate triple mutants. Furthermore, we generated *emf2-10 vrn2-1* lines with *STM::GUS*, *WUS::GUS*, and *LEAFY::GUS* reporter genes.

RNA extraction and RT–qPCR analysis

For quantitative reverse transcription–PCR (RT–qPCR) analysis, inflorescences were dissected and open flowers (older than stage 12) were removed (Smyth *et al.*, 1990). For harvesting of *35S::AP1-GR ap1-1 cal-1* samples, only the cauliflower structures of the main inflorescence were harvested. Leaf and pedicel tissue contamination was minimized by dissection as previously described (Engelhorn *et al.*, 2017). Samples were collected from non-induced *35S::AP1-GR ap1-1 cal-1* (t0) tissue and *35S::AP1-GR ap1-1 cal-1* 5 d after induction (t5, approximately floral stage 7) (Smyth *et al.*, 1990; Wellmer *et al.*, 2006). Total RNA of 3–6 biological replicates was extracted with TRIZOL (Invitrogen) and cDNA was synthesized using RevertAid reverse transcriptase (Thermo Fisher). Real-time RT–qPCR was performed by using SYBR Green I for LightCycler 480 (Roche). As internal control served *eIF4A* since its expression is unchanged during early flower development or in PcG mutants if normalized to *TIP41*, *RTFbox* (*AT5G15710*), or *UBQ10* (Supplementary Fig. S1; Wellmer *et al.*, 2006; Li *et al.*, 2020; Yan *et al.*, 2020; Sun *et al.*, 2021; Krizek *et al.*, 2021). The expression levels are expressed as the mean of relative fold changes of at least three biological replicates (values are scaled to the wild type or t0), and the error bars represent the SEM (Student's *t*-test); for $n \geq 4$, the trimmed mean is shown. The RT–qPCR primers used are listed in Supplementary Table S1.

RNA in situ hybridization

Non-radioactive *in situ* hybridizations with *CLV3*, *WUS*, *STM*, *AP3*, and *LFY* antisense probes were performed as previously described (Müller-Xing *et al.*, 2014). The *SVP* plasmid for generating antisense probes was kindly provided by Peter Huijser (Hartmann *et al.*, 2000).

ChIP assay and ChIP-Seq

ChIP assays were performed as described previously (Müller-Xing *et al.*, 2014). The chromatin was fragmented to an average length of 200–400 bp by sonication. We used the anti-tri-methylated histone H3K27 antibody (Abcam; ab6002). DNA was recovered by phenol:chloroform:isoamyl alcohol (25:24:1). Then, the DNA was analyzed by ChIP-qPCR; the primers used are listed in Supplementary Table S2. For ChIP-Seq analysis, the recovered DNA from the H3K27me3 ChIP experiment was combined in two biological replicas for each stage (*35S::AP1-GR ap1-1 cal-1*, t0 and t5). The ChIP-Seq assays were performed as described previously (Velanis *et al.*, 2016) and were carried out in the Glasgow Polyomics Facility (University of Glasgow).

ChIP-Seq analysis

The H3K27me3 ChIP-Seq reads were aligned to the *A. thaliana* genome TAIR10 using Bowtie2 with default parameters. Multimapping reads and PCR duplicates were discarded together with unmapped reads, leaving

only unique mapped reads for the downstream analysis. In order to retrieve the histone modifications patterns, peak calling was performed using MACS2 with the broad option and a *P*-value threshold set to 0.01 (Gaspar, 2018, Preprint). The differential methylation analysis was run using DiffBind with the DESeq2 method (*P*-value <0.05) (Stark and Brown, 2011). The differentially methylated regions were assigned to genes using the ChIPseeker package (Yu *et al.*, 2015). All those steps were performed using Curta, the High Performance Computing (HPC) of the Freie Universität Berlin (Bennett *et al.*, 2020). For each gene containing at least one differentially methylated region, a fold change was computed by counting the RPKM (reads per kilobase per million mapped reads) over the whole gene region [transcription start site (TSS) to transcription end site (TES)] in each condition using the featureCounts package and the RPKM function from edgeR (Liao *et al.*, 2014). The Spearman correlation analysis was performed in R Studio using the expression data from Ryan *et al.* (2015). All steps until the R part of the analysis were performed using Curta; the computing time was kindly provided by the HPC Service of ZEDAT, Freie Universität Berlin. In addition, Venny 2.1 (https://bioinfogp.cnb.csic.es/tools/venny/index.html) was used for comparisons of gene lists, and Integrative Genomic Viewer (IGV; Version2.3.88) was used for visualizing H3K27me3 pattern at gene loci to different time points.

GUS staining

Detection of β-glucuronidase (GUS) activity in tissue preparations were performed as described, with minor modifications (Li *et al.*, 2020). In brief, inflorescences with flowers were harvested and immersed in the GUS assay solution (50 mM $NaHPO_4$, 0.5 mM ferrocyanide, 0.5 mM ferricyanide, and 1% Triton X-100, pH 7.2) containing 1 mM X-Gluc. The tissues in the GUS solution were vacuum infiltrated for 30 min, and then incubated at 37 °C for ~3 h to overnight. To remove the chlorophyll, stained tissues were carried through ethanol series and then observed with a Nikon SMZ25 stereomicroscope.

Imaging

Photographs were taken with either a digital camera (Nikon D7200, Japan) or a dissecting microscope with a 5 mega pixel digital camera (Motic K-500L, China). Digital photographs and graphics were collated with PowerPoint or Adobe Photoshop and adjusted as described before (Müller-Xing *et al.*, 2014).

Results

Flowers with strong depletion of PcG activity feature increased size and indeterminacy of the floral meristems

In previous studies, we reported floral reversion in Arabidopsis lines with strongly depleted PcG activity, such as *emf2-10 vrn2-1* or *iCLF*, when shifted from inductive to non-inductive conditions, demonstrating that H3K27me3 is required to maintain floral commitment and IM identity (Müller-Xing et al., 2014, 2015). Flowers of *emf2-10 vrn2-1* and *iCLF* display diverse but similar developmental defects during flower development, indicating misregulation of a similar set of target genes (Müller-Xing *et al.*, 2014). The features of flowers with strongly depleted PcG activity include a low penetrance homeotic organ transformation and fused floral organs (Fig. 1D–L; Supplementary Fig. S2). In contrast, additional floral organs are the predominant phenotype of *emf2-10 vrn2-1* and *iCLF* flowers (Fig. 1A–F; Supplementary Fig. S2). The number of all floral organ types was increased, with the exception of stamens (Fig. 1I; Supplementary Fig. S2F). Supernumerary floral organs often are the result of an increased FM size (Müller *et al.*, 2008). Therefore, we measured the diameter of *emf2-10 vrn2-1* mutant FMs in longitudinal sections of floral primordia, stage 3–4. Like the vegetative SAM and IM (Fig. 2A–D), the FM size was significantly increased in *emf2-10 vrn2-1*, while the FM domes were rather higher than wider in comparison with the wild type (Supplementary Fig. S3). Thus, the extra carpels in flowers with strongly depleted PcG activity could be caused by the enlarged FMs.

The carpels of *emf2-10 vrn2-1* and *iCLF* flowers were normally fused to form a club-shaped silique (Fig. 1D, K–M). A small proportion of the siliques displayed incomplete valve fusion at their distal ends, which opened the view to a fifth whorl that was composed of ectopic carpels (Supplementary Fig. S2H). To test the frequency of fifth whorls in *emf2-10 vrn2-1* and *iCLF* flowers, we opened siliques with fused carpels (Fig. 1M) and found that 70–90% of the siliques contained a fifth whorl. Also, *clv* and *crn* mutants develop enlarged and indeterminate FMs causing club-shaped siliques with increased numbers of carpels and a fifth whorl (Clark et al., 1993, 1995; Kayes and Clark, 1998; Müller *et al.*, 2008) resembling siliques with strongly depleted PcG activity (Supplementary Figs S4, S5). Similar to *emf2-10 vrn2-1* and *iCLF*, *clv2* mutants exhibit flower to shoot transformation specifically under short-day growth conditions (Kayes and Clark, 1998; Müller-Xing et al., 2014, 2015). Furthermore, the morphology of the gynoecia in *emf2-10 vrn2-1* and *iCLF* flowers was occasionally altered, and the portion covered by valves was reduced (Supplementary Fig. S2D). This valveless phenotype is also associated with *clv* mutant siliques (Kayes and Clark, 1998; Diévart *et al.*, 2003). To summarize, increased carpel number, enlarged and indeterminate FMs that produce a fifth whorl, club shape, and valveless siliques are phenotypes of flowers with strongly depleted PcG activity shared with *clv* mutants.

PcG activity promotes determinacy of the floral stem cell pool in parallel to CLV3 *signaling and partially independent of* WUS *expression levels*

The enlarged size of the vegetative SAM, IM, and FMs, and the similarity of the silique phenotype in plants with strongly depleted PcG activity to that of *clv* mutants suggest that *CLV3* signaling and PcG function might act in a common genetic pathway to suppress *WUS* expression. To test this hypothesis, we analyzed the expression patterns of *CLV3*, which is an established stem cell marker (Fletcher *et al.*, 1999), and *WUS* in *emf2-10 vrn2-1* mutant flowers by RNA *in situ* hybridization and histochemical staining for *WUS::GUS* reporter gene activity (Fig. 2E–L). The *CLV3*

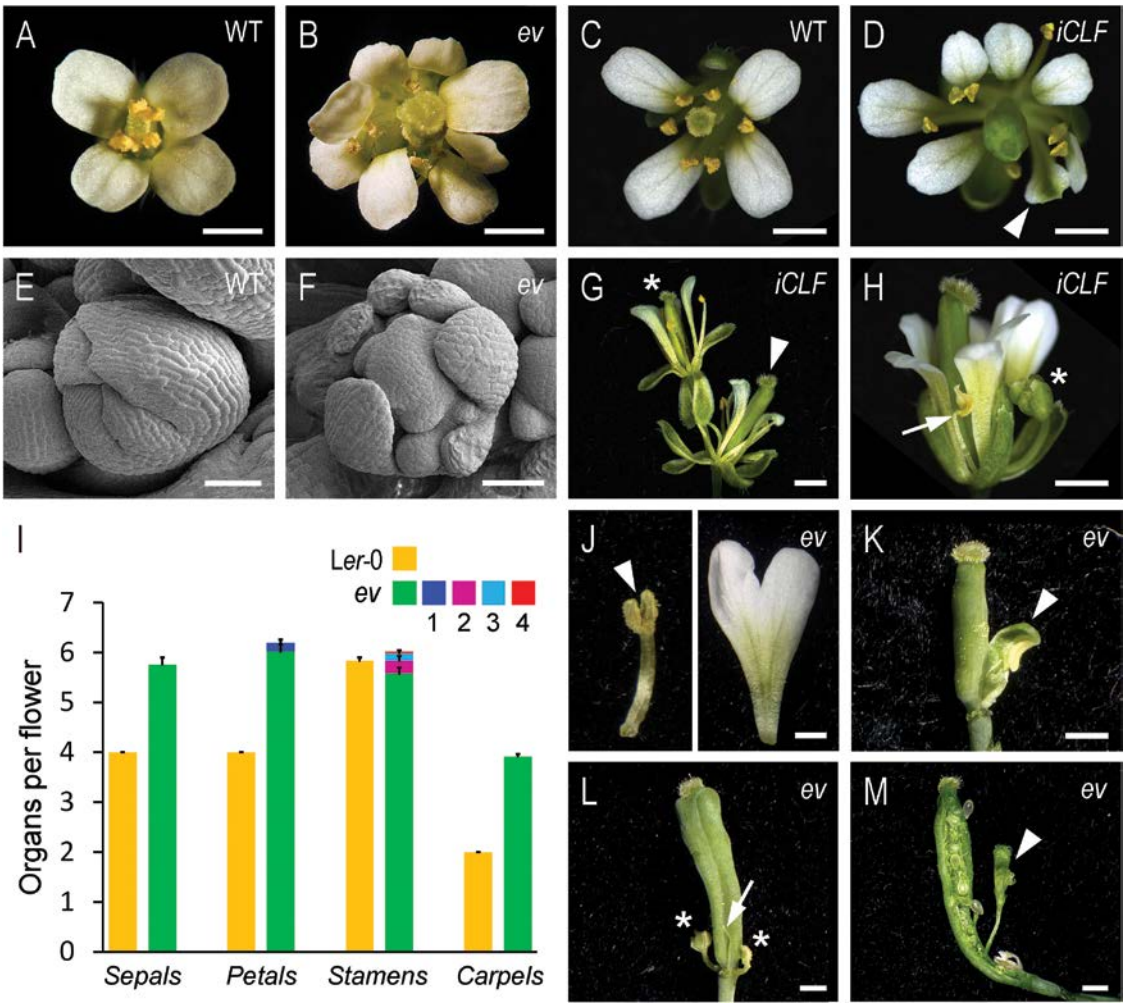

Fig. 1. Pleiotropic defects in flowers with strongly depleted PcG activity. (A–D) *emf2-10 vrn2-1* double mutant (*ev*) and *clf-28 swn-7 CLF-GR* (*iCLF*) flowers carrying extra floral organs including the well-visible petals in comparison with the wild-type [WT: L*er*-0 (A) and Col-0 (C)] flowers with four white petals. (D) Arrowhead indicates a sepaloid petal. (E and F) Scanning electron micrographs of Ws-0 (WT) and *ev* flowers stage 11–12 (Smyth *et al.*, 1990). Note that the sepals of *ev* are not closed. (G and H) *iCLF* flowers with petaloid stamen (arrow) and secondary flowers (asterisks) similar to *ap1* mutants; the arrowhead marks the primary flower. (I) Organ number in *ev* mutant flowers (green bars) compared with L*er*-0 flowers (orange bars) ±SEM (*n*=50). 1, dark blue: sepaloid petals; 2, purple: flower organs with mixed staminoid and sepaloid identity; 3, light blue: filament without anthers; 4, red: stamen-carpel fusion. (J) Left panel: two fused stamens (arrowhead). Right panel: two fused petals. (K) Third whorl carpel fused with an anther (arrowhead). (L) Silique with extra carpels after abscission of outer organs: two secondary flowers (asterisks) and one filament (arrow) are marked. (M) *ev* silique, organs of a fifth whorl are visible (arrowhead) after cutting the silique open. Note that the flowers in (A, B, I–M) are *er* mutant. All scale bars=1 mm, with the exception of (E and F)=100 µm.

expression domain appeared triangular in longitudinal sections of wild type meristems. In the enlarged *emf2-10 vrn2-1* IMs and FMs, *CLV3* was more strongly expressed in slightly expanded domains, indicating accumulation of more floral stem cells. Furthermore, *CLV3* expression was also temporally extended and maintained beyond stage 6 of flower development, consistent with the hypothesis that increased and prolonged stem cell activity induces the formation of a fifth whorl (Supplementary Fig. S5F). Although *WUS* is also expressed beyond flower stage 6 (Fig. 2K, L, P), the *WUS* expression domain in *emf2-10 vrn2-1* IMs and FMs appeared smaller and the staining weaker (Fig. 2G, H), suggesting that weaker *WUS* is not the reason but the consequence of increased *CLV3* expression.

In order to determine whether the *clv*-like phenotype of flowers with strongly depleted PcG activity might be due to lost or reduced activity of *CLV3* or of the CLV3 receptors, we combined *emf2-10 vrn2-1* with several *CLV3* signaling mutants. We examined the floral organ number in *clv3-2 emf2-10 vrn2-1* triple mutants and found that the carpel number was increased to 7.8 in comparison with 6.0 in *clv3-2* single mutants and 3.9 in *emf2-10 vrn2-1* double mutants (Fig. 2M–O, Q). Thus, *clv3-2* mutants strongly enhanced PcG double mutants, indicating that *CLV3* signaling and PcG proteins restrict the

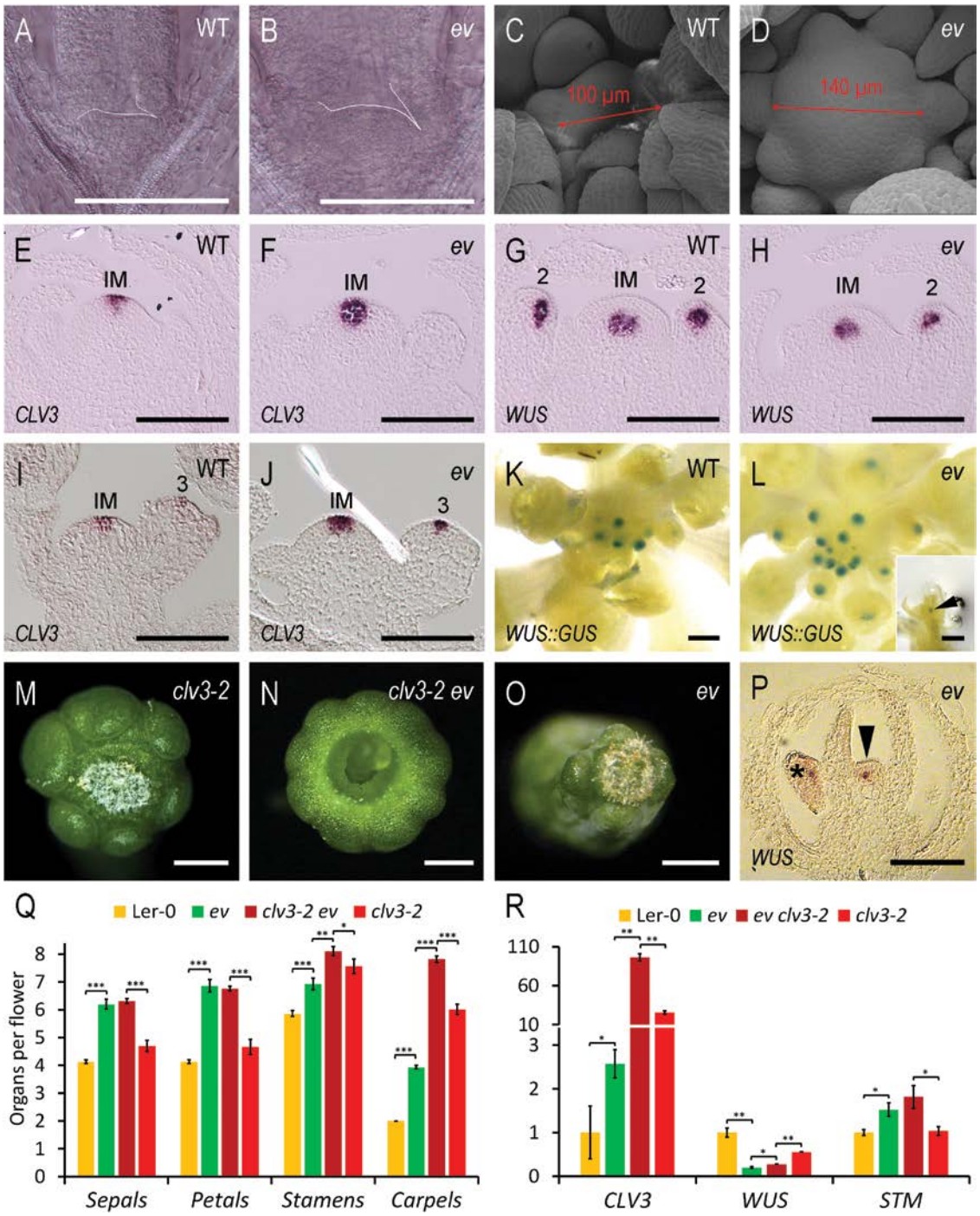

Fig. 2. Effects of strong PcG deficiency on meristem size and FM indeterminacy and genetic interaction with loss of *CLV3* function. (A–D) Increased meristem size of the vegetative SAM (A, B) and IM (C, D) in *emf2-10 vrn2-1* (*ev*) mutants in comparison with the wild type (WT: Ws-0). (E–J) *CLV3* and *WUS* RNA *in situ* hybridizations in *ev* mutant IM and FMs in comparison with the WT [Ws-0 (E, G) and La-0 (I)]. (K, L) *WUS::GUS* staining in L*er*-0 and *emf2-10 vrn2-1* (*ev*). (L) In the inset, the arrow indicates *WUS::GUS* expression in an *ev* flower with slotted gynoecial tube (floral stage ≥7; Smyth *et al.*, 1990). (M–O) Additive increase of ectopic carpels in *clv3-2 emf2-10 vrn2-1* (*clv3-2 ev*) triple mutants. (N) Note that tissue of the fifth whorl grew out the unfused carpels. (P) *WUS* RNA *in situ* hybridizations of *ev* flower, stage 9 (Smyth *et al.*, 1990). *WUS* is expressed in the indeterminate FM (arrow) and anthers (asterisk). (Q) Flower organs in *clv3-2 ev* triple mutants ±SEM; $n \geq 30$. (R) RT–qPCR analyses of gene expression in *clv3-2 ev* triple mutant inflorescence apices; columns indicate expression changes normalized by *elF4*, relative to expression in L*er*-0, ±SEM ($n=3$). All scale bars=100 µm, with the exception of (M–O)=1 mm.

number of carpels independently. Also, the valveless phenotype was enhanced in *clv3-2 emf2-10 vrn2-1* siliques (Supplementary Fig. S4). The analysis of *clv1-11 emf2-10 vrn2-1* and *crn-1 emf2-10 vrn2-1* triple mutants gave similar results (Supplementary Fig. S5). From this genetic analysis, we conclude that *CLV3* signaling and PcG proteins restrict the size and termination of FMs independently of one another.

We confirmed by RT–qPCR that *CLV3* is up-regulated in *emf2-10 vrn2-1* inflorescences and found synergistically enhanced *CLV3* expression (96.3× higher than the wild type) in *clv3-2 emf2-10 vrn2-1* triple mutants (Fig. 2R). This is in line with our carpel number analysis (Fig. 2Q), and the conclusion that *CLV3* signaling and PcG proteins control the floral stem cell population in parallel pathways. Similar to the stem cell marker *CLV3*, the meristem marker *STM* was up-regulated in *emf2-10 vrn2-1* (Fig. 2R). Notably, loss of *CLV3* had no significant effect on *STM* expression either in PcG-deficient or in wild-type plants, indicating that PcG activity but not *CLV3* signaling restricts *STM* expression. We also confirmed the down-regulation of *WUS* in *emf2-10 vrn2-1* inflorescences (Fig. 2R). Thus, we reasoned that the increased *CLV3* expression could cause the lower *WUS* expression, but we found only a partial rescue of *WUS* in *clv3-2 emf2-10 vrn2-1* triple mutants (Fig. 2R), suggesting the up-regulation of other *WUS* repressors in *emf2-10 vrn2-1*.

Our genetic analysis of flower phenotype and gene expression in *clv3-2 emf2-10 vrn2-1* triple mutants revealed that *CLV3* signaling and PcG proteins control the floral stem cell population in parallel pathways. Although *WUS* expression was temporally extended beyond floral stage 6 in PcG double mutants, *WUS* expression was lower in *emf2-10 vrn2-1* meristems. This finding suggests that the expansion of the stem cell domain is at least partially independent of *WUS* expression levels. It also gives rise to the possibility that PcG proteins control FM size and determinacy by repressing other meristematic regulators through H3K27me3 deposition.

Genome-wide analyses of changes in H3K27me3 levels after floral meristem determinacy

We reasoned that profiling of the dynamics of H3K27me3 accumulation rather than profiling the loss of H3K27me3 in unconditional PcG mutants could identify meristematic genes that are silenced by PcG proteins during early flower development. To investigate the dynamics of H3K27me3, we took advantage of the previously described *AP1-GR ap1-1 cal-1* floral induction system (Wellmer *et al.*, 2006), which can provide synchronized flower tissue of specific developmental stages (Fig. 3A, B). To assess the correlation of FM termination and changes of H3K27me3 levels, we chose floral primordia in stage 7 (t5, 5 d after induction with dexamethasone), which constitutes the earliest floral stage without meristematic tissue. We performed RT–qPCR and ChIP-qPCR to validate the t5 samples in comparison with the non-induced reference samples with IM tissue (t0). In wild-type inflorescences, *SVP* mRNA accumulates in floral primordia at stage 1 and 2 and is silenced in floral primordia during stage 3 (Fig. 3C). In the t5 samples, expression of the stem cell marker *CLV3* was reduced to background levels, indicating the presence of only post-meristematic tissue, while *SVP* mRNA levels were decreased to <3% of the mRNA levels in the t0 samples, whereas *SVP* H3K27me3 levels tripled (Supplementary Fig. S6). These data suggested that the tissues of the *AP1-GR ap1-1 cal-1* t0 and t5 samples were homogenous and the t5 sample showed synchronized and uniform floral induction, so we proceeded with the ChIP-Seq approach.

In floral stage 7 (t5), we identified 466 differentially methylated peaks corresponding to 420 differentially methylated genes (DMGs) including *SVP* (Fig. 3D–F). A total of 296 coding genes, three miRNAs, and five transposable elements significantly increased H3K27me3 levels in comparison with the controls (t0) (Fig. 3D). *OBO1* showed the highest increase in H3K27me3 levels (16.8-fold), while *OBO2* was the most heavily methylated H3K27me3 target gene at t5 (190.3 RPKM in Table 1 and Supplementary Table S5). On the other hand, chromatin loci of 110 coding genes, one miRNA, and five transposable elements had significantly decreased H3K27me3 levels in the t5 samples compared with the control (t0) samples (Fig. 3D). The strongest H3K27me3 reduction of all coding genes occurred at *SEP3* chromatin (Supplementary Fig. S8A, B; Supplementary Table S6), which encodes the most prominent E function cofactor for ABC-type MADS TFs (Pelaz *et al.*, 2001; Melzer *et al.*, 2009; Immink *et al.*, 2009; Lopez-Vernaza *et al.*, 2012; Hugouvieux *et al.*, 2018). Although *WUS* and *AG* were not among the DMGs identified by the ChIP-Seq, we confirmed by independent ChIP-qPCR experiments that the *WUS-AG* negative feedback loop was accompanied by reduced H3K27me3 levels at *AG*, whereas the *WUS* gene locus significantly gained H3K27me3 (Supplementary Fig. S9).

We compared our H3K27me3 datasets with published expression data (Ryan *et al.*, 2015). We found that changes of H3K27me3 and expression levels were highly negatively correlated (Fig. 4A–C). In further comparison, we identified 151 coding genes that significantly gained H3K27me3 and had decreased expression rates, whereas 49 loci lost H3K27me3 and increased expression accordingly (Fig. 4D, E; Supplementary Fig. S10; Supplementary Table S5, S6). To verify our ChIP-seq data and the published expression data, we performed ChIP-qPCR and RT–qPCR for some TF genes of interest on independent *AP1-GR ap1-1 cal-1* t0 and t5 samples (Supplementary Fig. S8). Notably, TFs were highly over-represented (40.4% and 26.5%) within the genes that showed a negative correlation between changes in gene expression and changes in H3K27me3 (Fig. 4D, E). The majority of the genes, which are targeted by these H3K27me3-regulated TFs, are not H3K27me3 targets (Supplementary Fig. S11). This suggests that regulation by H3K27me3 is part of an epigenetic switch, which stabilizes the expression changes of a few hundred TFs that, in turn, control transcriptional changes of thousands

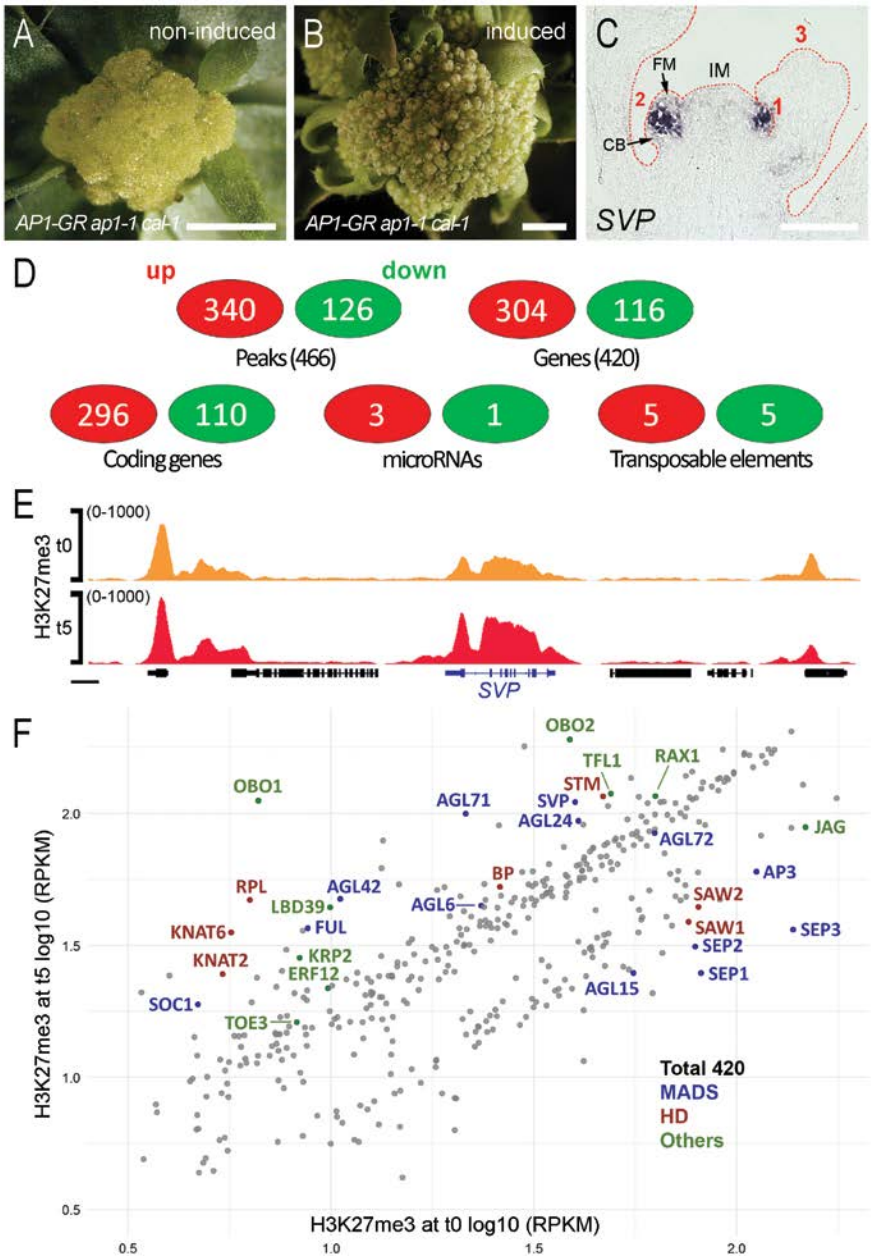

Fig. 3. Genome-wide changes of H3K27me3 levels during early flower development. (A, B) The *AP1-GR ap1-1 cal-1* system (Wellmer *et al.*, 2006) provides an enormous amount of either undifferentiated inflorescence meristem (A, non-induced) or synchronized flower tissue (B, induced). (C) *SVP* RNA *in situ* RNA hybridization in a wild-type inflorescence grown under long-day conditions. *SVP* is expressed throughout stage 1 floral primordia (1) whereas in stage 2 flower primordia (2), the *SVP* expression domain divides the flower meristem (FM) and cryptic bract (CB). Note that *SVP* is not expressed in flower primordia stage 3 or older; IM, inflorescence meristem. (D–F) *AP1-GR ap1-1 cal-1* ChIP-Seq data. (D) Number of differentially methylated peaks (identified by DiffBind) and gene loci (identified by ChIPseeker) encoding proteins, miRNAs, or transposable elements. The differentially methylated peaks and genes are listed in Supplementary Table S3 and S4, respectively. A cluster analysis (DiffBind) can be found in Supplementary Fig. S7. (E) Close-up of the genomic region containing the *SVP* locus (blue). H3K27me3 levels at *SVP* increased significantly, whereas neither of the neighboring H3K27me3 target sites showed significant changes. (F) Comparison of all H3K27me3 target genes that are differentially methylated in IMs (t0) and flowers, stage 7 (t5). Each point represents an H3K27me3-enriched gene. ChIP-Seq data were normalized to RPKM. Genes encoding MADS domain TFs (blue), homeodomain (HD) TFs (red), or other proteins of interest (green) are indicated.

of genes that are largely not H3K27me3 targets. Furthermore, the three miRNA genes *MIR2111B*, *MIR319A*, and *MIR165B* gained H3K27me3 (Fig. 3D; Supplementary Table S7), indicating indirectly positive regulation of coding genes by H3K27me3-mediated repression of miRNA genes during early flower development (Lafos *et al.*, 2011).

Table 1. Selection of TF genes, encoding known or putative floral meristem regulators, which gained H3K27me3 and were significantly reduced in expression during FM arrest

Gene Annotation		H3K27me3 (RPKM)		
Gene ID	**Name**	**t0**	**t5**	**FC**
(A) HD TF genes				
AT5G02030	*PENNYWISE* (*PNY/BLR/RPL*)	**6.3 ± 0.4**	**46.9 ± 2.2**	**7.4**
AT1G23380	*KNOTTED-like* from *Arabidopsis thaliana 6* (*KNAT6*)	**5.7 ± 0.1**	**35.4 ± 4.3**	**6.2**
AT1G70510	*KNOTTED-like* from *Arabidopsis thaliana 2* (*KNAT2*)	**5.4 ± 0.2**	**24.6 ± 2.5**	**4.5**
AT1G62360	*SHOOT MERISTEMLESS* (*STM*)	**46.9 ± 1.3**	**116.0 ± 2.0**	**2.5**
AT2G27990	*POUND-FOOLISH* (*PNF/BLH8*)	**8.7 ± 0.3**	**21.3 ± 0.6**	**2.4**
AT4G08150	*BREVIPEDICELLUS* (*BP/KNAT1*)	**26.1 ± 1.3**	**52.7 ± 3.6**	**2.0**
AT5G41410	*BELL 1* (*BEL1*)	**50.1 ± 0.1**	**78.9 ± 0.7**	**1.6**
AT2G33880	*STIMPY* (*STIP/WOX9*)	**94.2 ± 2.4**	**136.3 ± 2.7**	**1.4**
(B) MADS TF genes				
AT5G62165	*FOREVER YOUNG FLOWER* (*FYF/AGL42*)	**10.5 ± 0.3**	**47.3 ± 6.3**	**4.5**
AT5G60910	*FRUITFULL* (*FUL/AGL8*)	**8.8 ± 0.7**	**36.8 ± 4.0**	**4.2**
AT2G45660	*SUPPRESSOR OF OVEREXPRESSION OF CONSTANS 1* (*SOC1/AGL20*)	**4.7 ± 0.2**	**18.9 ± 3.7**	**4.0**
AT2G22540	*SHORT VEGETATIVE PHASE* (*SVP/AGL22*)	**40.0 ± 2.1**	**110.2 ± 14.4**	**2.8**
AT4G24540	*AGAMOUS-LIKE 24* (*AGL24*)	**40.7 ± 3.5**	**93.7 ± 7.3**	**2.3**
AT1G26310	*CAULIFLOWER* (*CAL/AGL10*)	**44.2 ± 0.1**	**73.7 ± 10.6**	**1.7**
AT5G51860	*AGAMOUS-LIKE 72* (*AGL72*)	**62.7 ± 0.2**	**84.1 ± 8.7**	**1.3**
(C) Other TFs				
AT2G31160	*ORGAN BOUNDARY 1* (*OBO1/LSH3*)	**6.6 ± 0.2**	**111.5 ± 11.1**	**16.8**
AT5G28490	*ORGAN BOUNDARY 2* (*OBO2/LSH1*)	**38.8 ± 0.5**	**190.3 ± 18.9**	**4.9**
AT5G03840	*TERMINAL FLOWER1* (*TFL1*)	**49.0 ± 0.4**	**118.7 ± 11.2**	**2.4**
AT4G35900	*FD* (*ATBZIP14*)	**4.5 ± 0.5**	**9.7 ± 0.2**	**2.2**

Selection of TF genes that were gaining H3K27me3 (ChIP-Seq) and significantly reduced in expression (Ryan *et al.*, 2015) during early flower development. The complete data for 151 genes are listed in Supplementary Table S5. FC, fold change (t5/t0: floral stage 7-IM).

To determine whether TF genes could contribute to the floral indeterminacy and other phenotypes in flowers with strongly depleted PcG activity, we examined the expression and H3K27me3 levels of several TFs in *emf2-10 vrn2-1* mutant inflorescences using RT–qPCR and ChIP-qPCR. Independent of whether they had increased or decreased H3K27me3 levels during early flower development, the majority of the tested TF genes (93.3%) lost H3K27me3 in *emf2-10 vrn2-1* (Supplementary Fig. S12). Within the TF genes that gained H3K27me3 and decreased expression in *AP1-GR ap1-1 cal-1* (t5–t0), we identified eight HD (seven TALE and one WOX) and seven MADS TF genes (Fig. 4F; Table 1). Surprisingly, only five of the eight HD TFs and four of the seven MADS TFs were up-regulated in the PcG double mutants, whereas one MADS and two HD TF genes were down-regulated (Supplementary Fig. S13). Thus, only 60% of the HD and MADS TF genes, whose H3K27me3 levels increased during early flower development, were up-regulated in strongly PcG-deficient flowers, while the down-regulation of three TF genes indicates that PcG proteins can indirectly promote their expression.

PcG proteins promote FM identity and determinacy by silencing AGL24 *that encodes a repressor of ABCE function genes and* STM

The FM identity genes *LFY* and *AP1* directly up-regulate each other in a positive feedback loop, and control the expression of floral homeotic MADS box genes (Kaufmann *et al.*, 2010; Wagner *et al.*, 1999; Moyroud *et al.*, 2011). As expected, we found *AP3* and *SEP3* within the 49 coding genes which significantly lost H3K27me3 and increased expression rates during early flower morphogenesis (Supplementary Fig. 8A; Supplementary Table S6). To determine if loss of PcG activity promotes the expression of ABCE-type MADS box genes, we performed RT–qPCR with *emf2-10 vrn2-1* inflorescence tips. Surprisingly, the expression of *AP1*, *AP3*, *PI*, *AG*, and *SEP3* was significantly reduced (Fig. 5A). Lower expression of *LFY* could explain the reduced expression rates of its target genes, but *LFY* was more highly expressed (Fig. 5A; Supplementary Fig. S14). An alternative possibility is that genes which encode repressors of the ABCE genes were up-regulated by strong depletion of PcG activity.

During the onset of flower development, *TFL1*, which encodes a repressor of *AP1*, is excluded from emerging floral primordia (Liljegren *et al.*, 1999; Ratcliffe *et al.*, 1999). The *TFL1* gene locus significantly gains H3K27me3 levels in 2 d (t2) (Engelhorn *et al.*, 2017), which developed to robust changes (t5; Supplementary Fig. S8D, E). Notably, the *FD* locus, encoding a bZIP TF that interacts with TFL1 to promote IM fate, also gained H3K27me3 (t5; Table 1). To test the significance of H3K27me3 accumulation, we performed RT–qPCR and found that *TFL1* was strongly up-regulated in *emf2-10 vrn2-1* inflorescences (Fig. 5A). Up to 15% of *emf2-10 vrn2-1* and *iCLF* flowers carry secondary flowers in the axils of leaf-like sepals (Fig. 1G, H, L), which is a phenotype firstly associated with *ap1*

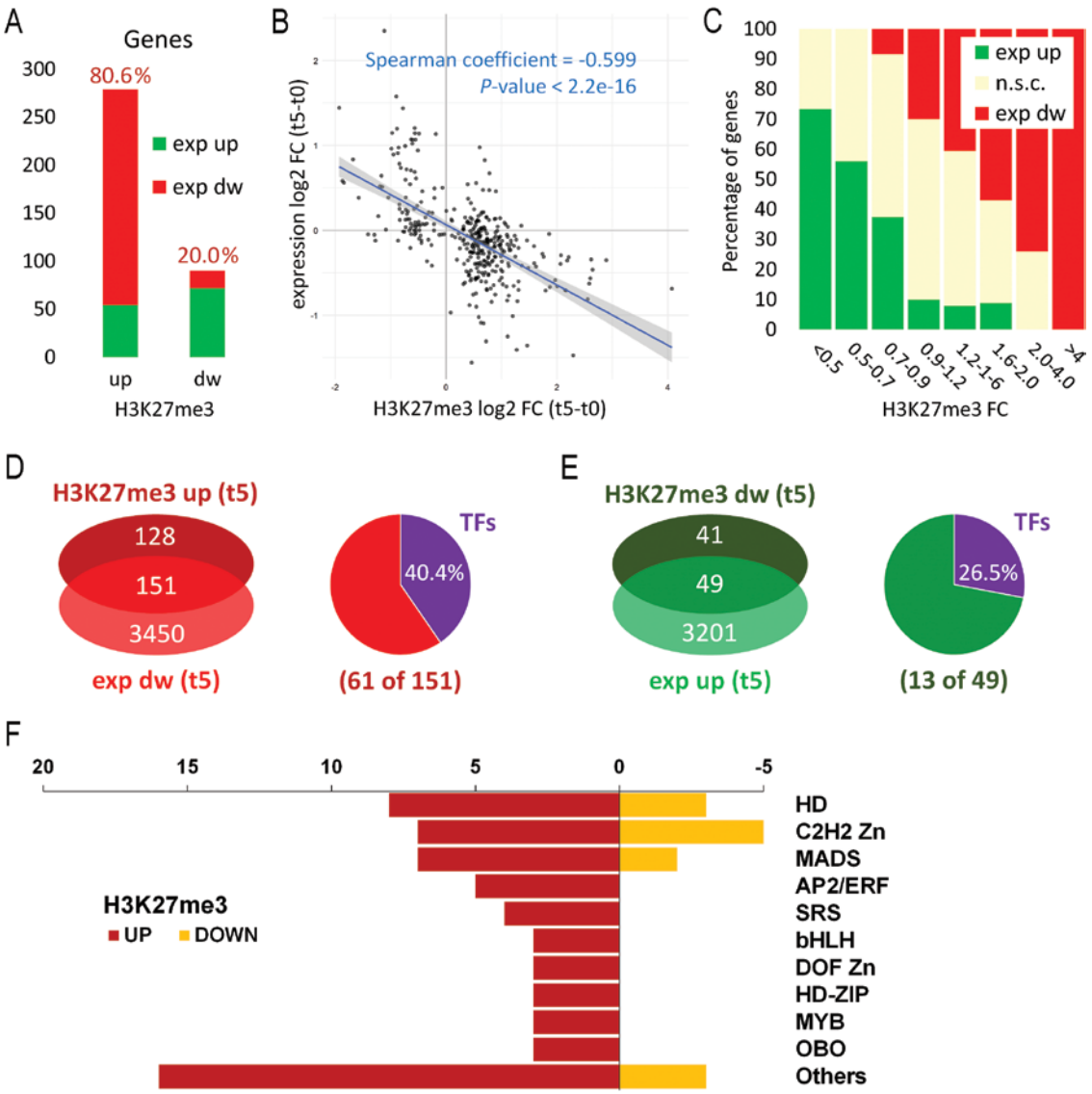

Fig. 4. Correlation of genome-wide changes in H3K27me3 levels and gene expression during early flower morphogenesis. (A–C) Correlation of DMGs and gene expression (Ryan *et al.*, 2015). (A) Bar diagram of all DMGs sorted by gain (up) and loss (dw) of H3K27me3. (B) Spearman correlation graph. (C) The DMGs are sorted by fold change of H3K27me3 levels. Numbers in each fold change (FC) category are indicated. (D, E) Venn diagrams (left) presenting the overlap of all coding genes with significant changes in H3K27me3 levels and gene expression (Ryan *et al.*, 2015). Pie charts (right) presenting the over-representation of transcription factors (TFs) in the groups of overlap. (F) Distribution of TFs, with significantly changed H3K27me3 and anti-correlation in expression, sorted by TF gene families. FC, fold change; exp, expression; dw, down; n.s.c., not significantly changed.

A-function mutant flowers, indicating partial reversion of FMs to IMs (Supplementary Fig. S15A–C) (Coen and Meyerowitz, 1991; Irish and Sussex, 1990). Therefore, the *ap1*-like phenotype could be caused by reduction of *AP1* expression by increased *TFL1*. However, the phenotype of *ap1* mutant flowers also includes loss of most petals, but *emf2-10 vrn2-1* and *iCLF* flowers carry rather more petals, although some *iCLF* flowers had fewer petals (Fig. 1A–D, I; Supplementary Fig. S2B). To determine to what extent the *ap1*-like phenotype in *emf2-10 vrn2-1* flowers is attributable to decreased levels of *AP1* mRNA, we generated *ap1-1 emf2-10 vrn2-1* triple mutants. The percentage of secondary flowers in the axis of first whorl organs was significantly increased in *ap1-1 emf2-10 vrn2-1* mutant flowers compared with *ap1-1* single mutants, indicating at least one *AP1*-independent pathway (Supplementary Fig. S15A–F).

Overexpression of the AP1 downstream target *AGL24* causes *ap1*-like and indeterminate flowers (Yu *et al.*, 2004) similar to the defects observed in *emf2-10 vrn2-1* mutant flowers (Fig. 5B–D). Indeed, *AGL24* was the most up-regulated gene of all key floral regulators that we tested in *emf2-10 vrn2-1* mutant inflorescences, whereas H3K27me3 levels were strongly

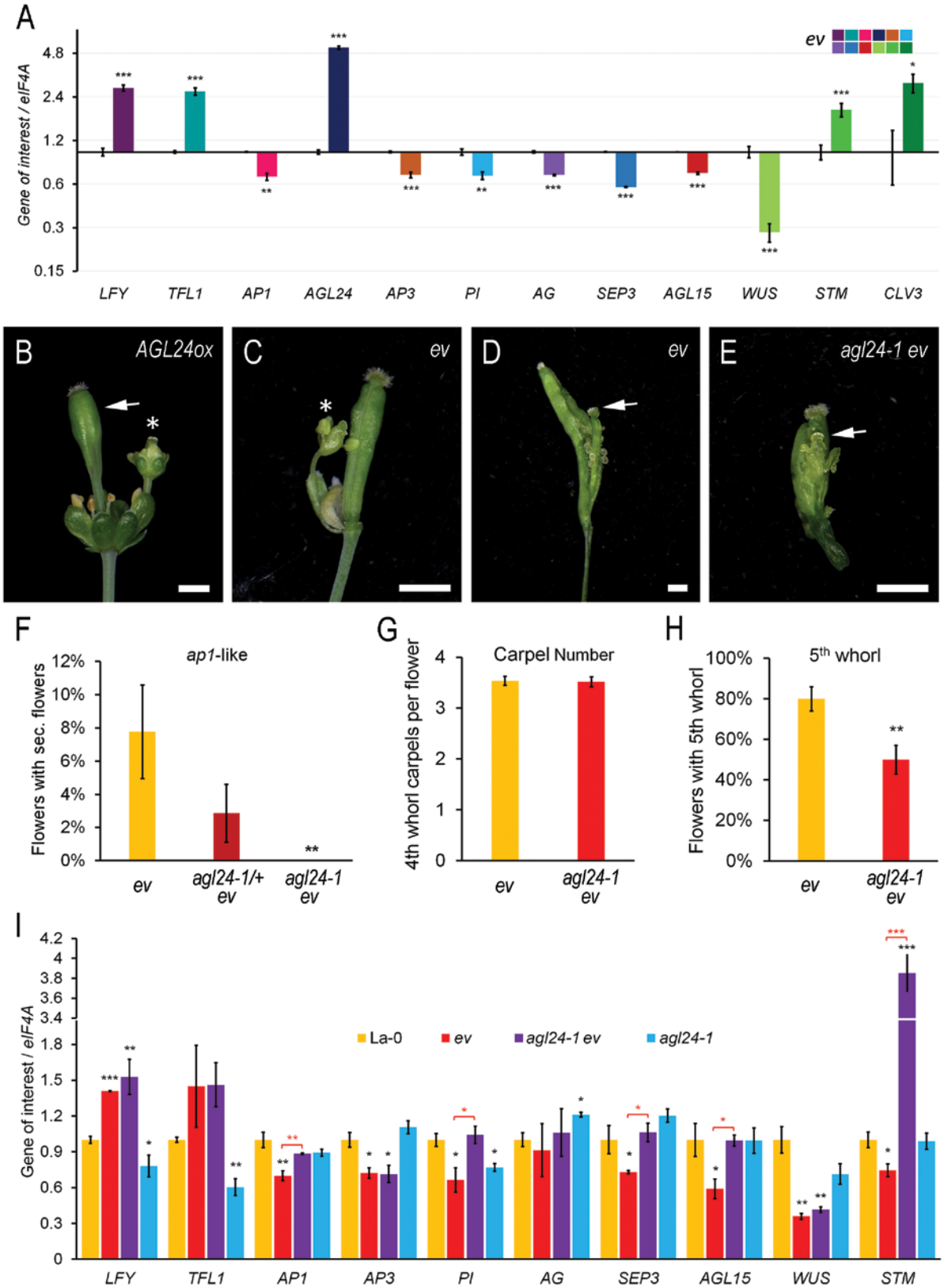

Fig. 5. Misexpression of *AGL24* represses several PcG target genes partially causing FM reversion and indeterminacy in PcG mutants. (A) RT–qPCR analyses of gene expression of TFs and *CLV3* in *emf2-10 vrn2-1* florescence apices; columns indicate expression changes in *emf2-10 vrn2-1* normalized by *eIF4A*, relative to expression in L*er*-0. Note the logarithmic scale. (B) Overexpression of *AGL24* results in indeterminate flowers carrying swollen siliques

reduced at the *AGL24* gene locus (Fig. 5A; Supplementary Figs S12B, S16). Although the expression of *TFL1* increased in *ap1-1 emf2-10 vrn2-1* mutant inflorescences, the loss of *AP1* did not significantly enhance *AGL24* expression in the PcG double mutants, suggesting that the strong up-regulation of *AGL24* is a direct result of the loss of H3K27me3 at the *AGL24* locus rather than an indirect result of reduced *AP1* expression (Supplementary Fig. S15G). Furthermore, *AGL24* expression was also increased in *iCLF* inflorescences and *clf swn* callus-like tissue (Supplementary Fig. S17). These findings indicate that increased *AGL24* activity could cause ectopic secondary flowers and FM indeterminacy in flowers with strongly depleted PcG activity. To test this hypothesis, we generated *emf2-10 vrn2-1* lines segregating *agl24-1*. We found full suppression of the *ap1*-like phenotype in homozygous *agl24-1 emf2-10 vrn2-1* flowers, whereas 2.9% of *agl24-1/+ emf2-10 vrn2-1* flowers and 7.8% of *emf2-10 vrn2-1* flowers carried at least one secondary flower (Fig. 5F). In contrast, the carpel number was not affected, while the percentage of flowers with a fifth whorl decreased in *agl24-1 emf2-10 vrn2-1* triple mutant flowers (Fig. 5G, H). These results suggest that *AGL24* misexpression is the main cause of *ap1*-like flowers and contributes to the fifth whorl, but has no effect on FM size or carpel number in plants with strongly depleted PcG activity. *AGL24*, *SOC1*, and *SVP* redundantly prevent ectopic expression of *AP3*, *PI*, *AG*, and *SEP3* in the floral anlagen in the IM and in emerging FMs before stage 3 (Gregis et al., 2006, 2009; Liu *et al.*, 2009). Hence, the strong up-regulation of *AGL24* could be one of the key factors that are involved in the decrease of *AP1*, *AP3*, *PI*, *AG*, and *SEP3* expression (Fig. 5A) and therefore the ABC function-related homeotic transformation in flowers with strongly depleted PcG activity. To obtain additional evidence for this conclusion, we examined the expression in the inflorescences of *emf2-10 vrn2-1* double and *agl24-1 emf2-10 vrn2-1* triple mutant plants using RT–qPCR (Fig. 5I). Consistent with the hypothesis that *AGL24* overexpression directly causes the down-regulation of the MADS TFs, the expression of *AP1*, *PI*, *SEP3*, and their target *AGL15* was rescued to wild-type levels, whereas *AP3* and *AG*, but also up-regulated TF genes such as *LFY* and *TFL1*, were unchanged. This indicates that *AGL24* misexpression causes the down-regulation of a subset of the TF genes that are down-regulated in PcG double mutant flowers. Surprisingly, *STM* expression was synergistically increased in *agl24-1 emf2-10 vrn2-1* triple mutants (Fig. 5I). Thus, although *AGL24* promotes FM indeterminacy (Yu *et al.*, 2004), *AGL24* acts redundantly with PcG proteins to prevent *STM* misexpression.

PcG proteins control FM activity by restriction of STM *expression*

STM is a well-known pluripotency gene belonging to the group of HD TF genes that gained H3K27me3 during FM determinacy (Table 1). As in *emf2-10 vrn2-1*, we found increased *STM* mRNA levels in *iCLF* inflorescences and *clf-28 swn-7* callus-like tissue (Fig. 5A; Supplementary Fig. S17). To determine the spatiotemporal expression patterns of *STM* in PcG double mutant flowers, we analyzed *STM* expression in *emf2-10 vrn2-1* by RNA *in situ* hybridization and histochemical staining for *STM::GUS* reporter gene activity (Fig. 6A–D). *STM* was more strongly expressed in *emf2-10 vrn2-1* floral primordia than in the wild type, and, like *WUS*, temporally extended beyond floral stage 6. This finding suggests that the ectopic expression of *STM* in the indeterminate FMs contributes to the fifth whorl in flowers with strongly depleted PcG activity. Furthermore, increased *STM* activity could cause the enlarged FMs and extra floral organ numbers in H3K27me3-deficient flowers. To test this hypothesis, we combined the strong *STM* allele *bum1-3* with *emf2-10 vrn2-1* and *iCLF*, constructing two lines with strongly depleted *STM* and PcG activity (Fig. 6I; Supplementary Fig. S18). Loss of *STM* affects the four floral whorls differently. While the total number of flower organs was reduced and all carpels lost, *bum1-3* flowers also displayed homeotic transformations of petals. The increased numbers of sepals were nearly rescued to the wild type level in *bum1-3 emf2-10 vrn2-1* and *bum1-3 iCLF* flowers, suggesting that increased *STM* activity contributes to the enlarged FM in the early stages of flowers with strongly depleted PcG activity. Loss of *STM* also rescued the increased carpel number in the strongly H3K27me3-deficient flowers of *bum1-3 iCLF* and *bum1-3 emf2-10 vrn2-1* triple mutants. Importantly, neither *bum1-3 iCLF* nor *bum1-3 emf2-10 vrn2-1* triple mutant flowers carried any fifth whorl structures (Supplementary Table S9). Similarly, loss of *WUS* resulted in premature arrest of FM activity in *wus-1 emf2-10 vrn2-1* mutant flowers, indicated by lack of most central floral organs (Fig. 6J). These findings indicate that *WUS* and *STM* activity are essential for FM indeterminacy in flowers with strongly depleted PcG activity.

Discussion

H3K27me3-mediated gene silencing by PcG proteins has been implicated in a wide variety of developmental processes in Arabidopsis, including leaf differentiation and termination of *WUS* during FM arrest (Lafos *et al.*, 2011; Liu *et al.*, 2011;

with a fifth whorl inside (arrow) and *ap1*-like secondary flowers (asterisk). (C) Most *ev* flowers carry a fifth whorl, and a few of them display *ap1*-like flowers (asterisk). (D, E) *emf2-10 vrn2-1* (*ev*) and *agl24-1 emf2-10 vrn2-1 (agl24-1 ev)* siliques. The arrows mark the dissected fifth whorl carpels. (F) Percentage of the *ap1*-like flower phenotype in *ev*, *agl24-1/+ ev*, and *agl24-1 ev* ($n \geq 70$). (G) Carpel number in *ev* and *agl24-1 ev* ($n=50$). (H) Percentage of flowers with a fifth whorl in *ev* and *agl24-1 ev* ($n=50$). (I) RT–qPCR analyses of gene expression in the *agl24-1 ev* triple mutant in comparison with *ev* double mutant inflorescence apices; columns indicate expression levels normalized by *elF4*, relative to expression in La-0. (A, I) All RT–qPCR experiments were performed with at least three biological replicates. (A, F, H, I) Asterisks indicate significant changes (Student's *t* test: $*P \leq 0.05$; $**P \leq 0.01$; $***P \leq 0.001$). All scale bars=1 mm.

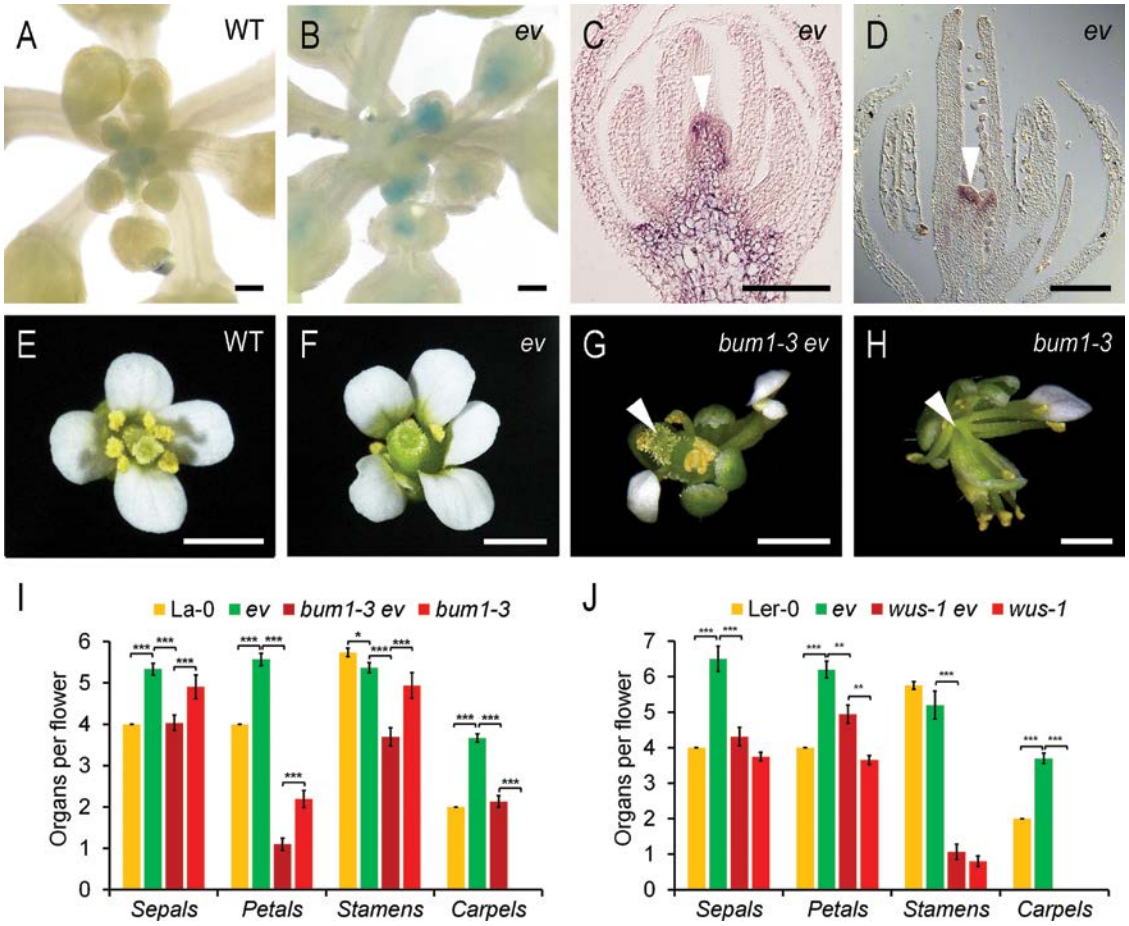

Fig. 6. *STM* contributes to FM indeterminacy in PcG mutants. (A, B) *STM::GUS* staining of the wild type (WT; L*er*-0) and *emf2-10 vrn2-1* (scale bars=0.1 mm). (C, D) RNA *in situ* hybridizations of *emf2-10 vrn2-1* flowers with *STM*. In contrast to the WT, FMs of *emf2-10 vrn2-1* mutants remain indeterminate after stage 6. *STM* expression (arrowheads) in indeterminate FM, floral stage 10 (C), and floral stage 15 (D). (E–I) Flower organs in *bum1-3 ev* triple mutants ±SEM ($n \geq 30$). (J) Flower organs in *wus-1 ev* triple mutants ±SEM ($n \geq 14$). Asterisks indicate significant changes (Student's *t*-test: $*P \leq 0.05$; $**P \leq 0.01$; $***P \leq 0.001$). Scale bars=100 μm (A–D) and 1 mm (E–H).

Sun *et al.*, 2019). However, the significance of increasing H3K27me3 levels for silencing of other developmental genes during floral organ morphogenesis and termination of the floral stem cell population remained widely unexplored. Here we reveal new insights into the function of PcG proteins that restrict expression of their direct targets and promote gene expression indirectly by repressing transcriptional repressors in the gene regulatory network of TFs that controls early flower development (Fig. 7).

PcG proteins indirectly activate floral regulator genes by silencing of their upstream repressors such as AGL24

In multicellular eukaryotes, including plants, H3K27me3 plays a fundamental role in the epigenetic regulation of tissue-specific expression patterns, which silences its direct targets and promotes gene expression indirectly by repressing miRNA genes (Lafos *et al.*, 2011; Shivram *et al.*, 2019). Although it has been implicated that PcG proteins can indirectly activate their own expression during seed development (Baroux *et al.*, 2006), we provide here genetic evidence that PcG proteins indirectly activate TF genes by silencing of upstream transcriptional repressors. One-third of the tested HD and MADS TF genes, although they lost the repressive H3K27me3 mark, were down-regulated or their expression was not changed in *emf2-10 vrn2-1* double mutants (Supplementary Fig. S13). In particular, the down-regulation of ABCE-type MADS genes indicates that PcG proteins can indirectly promote gene expression (Fig. 7). Among the MADS TF genes that showed the expected expression increase, we found *AGL24* mRNAs strongly accumulated. Several AGL24 target genes are known. At the onset of flower development, AGL24 acts redundantly with SVP, SOC1, and SEP4 to repress the expression of *TFL1*, while AGL24 forms heterodimers with AP1 that, redundantly with SVP–AP1 dimers, directly prevent premature expression of BCE-type MADS TF genes (Gregis et al., 2006, 2009; Liu *et al.*, 2013). Furthermore, SVP and AGL24 are direct positive

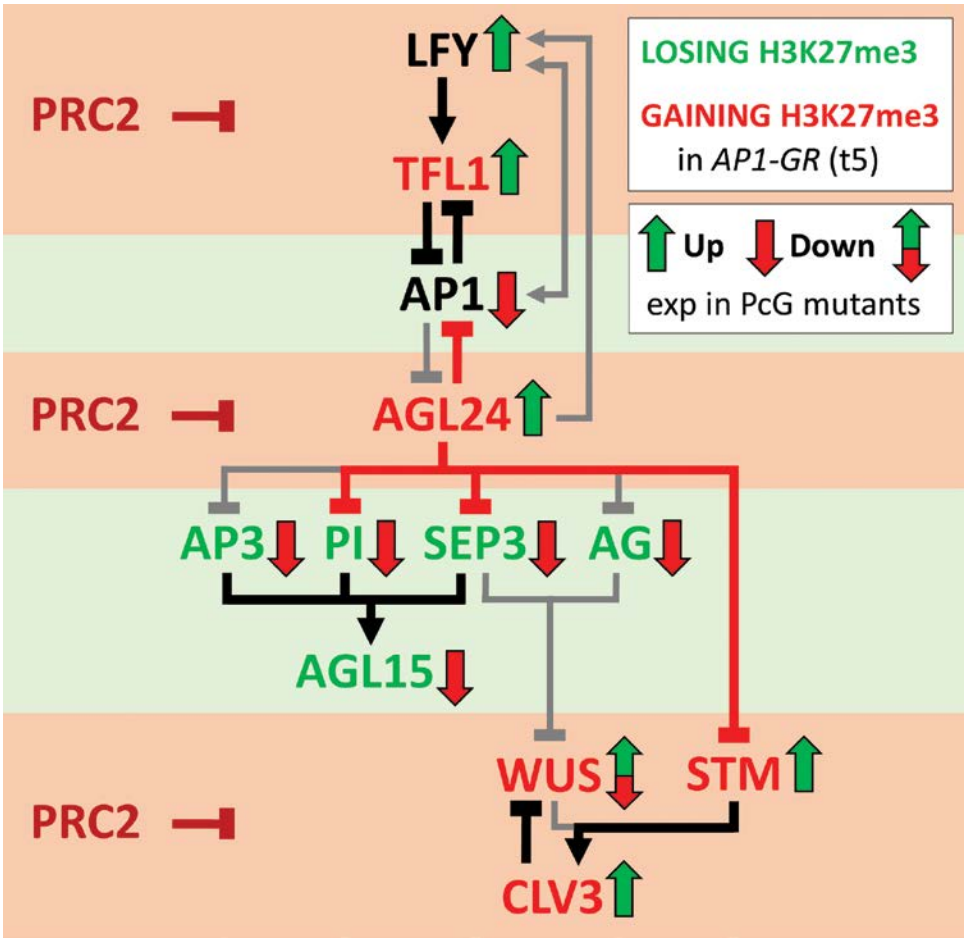

Fig. 7. Concept of epigenetic (co-)regulation of the floral gene regulatory network of TFs by PRC2 (H3K27me3). Hierarchic model of the gene regulatory network with alternating regulation levels of gene silencing by PRC2 activity and gene activation during early flower development. Note that PRC2 activity can indirectly activate genes by silencing of transcriptional repressors such as TFL1 and AGL24. Arrows, transcriptional activation. Arrows with blunt ends represent repression. Red arrows with blunt ends indicate repression by AGL24 in flowers with strongly depleted PcG activity. Gray arrows represent known transcriptional regulation in the wild type, which was suppressed in the strongly PcG-deficient background. Framed arrows: green, up-regulated expression, and red, down-regulated expression in *emf2-10 vrn2-1* double mutants (PcG). Note that although *WUS* expression is reduced in strongly PcG-deficient IMs and FMs, its expression is prolonged in the indeterminate FMs.

regulators of *LFY* and *AP1* in FMs (Grandi *et al.*, 2012). Although we could not confirm all of these transcriptional relationships in a strongly PcG-deficient background, we found correlation between ectopic *AGL24* activity and decreased expression of *AP1*, *PI*, *SEP3*, and *AGL15*, which was rescued in *agl24-1 emf2-10 vrn2-1* triple mutants (Fig. 5I). These findings are consistent with the hypothesis that PcG proteins silence *AGL24* but also other floral repressor genes to prevent the down-regulation of several flower development genes (Fig. 7).

Ectopic AGL24 *expression results in* ap1*-like floral reversion in* emf2-10 vrn2-1 *mutants and might contribute to other reversion phenotypes in plants with strongly depleted PcG activity*

Overexpression of *AGL24* causes an *ap1*-like floral reversion phenotype with ectopic flowers in the axil of first whorl organs and FM indeterminacy that is not a characteristic of *ap1* mutants (Irish and Sussex, 1990; Yu *et al.*, 2004; Liu *et al.*, 2007). Therefore, we concluded that high expression of *AGL24* at least partially causes the *ap1*-like floral reversion and FM indeterminacy in flowers with strongly depleted PcG activity, which we confirmed by genetic and expression analysis (Fig. 5). In PcG double mutants, the partial loss of flowering commitment results in different types of floral reversion including ectopic inflorescences inside siliques (Müller-Xing *et al.*, 2014, 2015). Remarkably, overexpression of *AGL24* can result in similar FM to IM reversion independently of the daylength condition (Yu *et al.*, 2004). With the exception of the *ap1*-like phenotype, *emf2-10 vrn2-1* mutants display floral reversions only under non-inductive short-day conditions (Müller-Xing *et al.*, 2014, 2015). Thus, the ectopic expression of *AGL24* is not sufficient for FM to IM reversion in *emf2-10 vrn2-1* mutants (at least in long days). Previously, we showed that the

activities of two other MADS TF genes, *FLC* and *SVP*, are critical for the floral reversion in *emf2-10 vrn2-1* mutants under non-inductive conditions, whereas ectopic *FLC* represses *FT* that is required for maintaining the commitment to flowering (L. Liu *et al.*, 2014; Müller-Xing *et al.*, 2014). Notably, the previous genetic analysis revealed that at least one other PcG target is involved (Müller-Xing *et al.*, 2014), and *AGL24* is a good candidate to act in parallel with *FLC* and *SVP* to promote daylength-dependent floral reversion in PcG double mutants.

PcG proteins promote FM determinacy by silencing of several floral regulators including AGL24 *and the pluripotency genes* WUS *and* STM

Flower development requires initiation, maintenance, and determinacy of the FM. The *CLV3–WUS* feedback loop appears to be an intertwined and inseparable machinery that controls the size of the OC (marked by *WUS* expression) and stem cell domain (marked by *CLV3* expression), which maintains all shoot meristems (Brand *et al.*, 2000; Schoof *et al.*, 2000). Most studies of FM determinacy focused on the direct or indirect transcriptional and epigenetic silencing of *WUS* in floral stage 6 (Lenhard *et al.*, 2001; Lohmann *et al.*, 2001; Zhao *et al.*, 2007; Sun et al., 2009, 2014, 2019; Ji *et al.*, 2011; X. Liu *et al.*, 2011, 2014; Yumul *et al.*, 2013; Huang *et al.*, 2017; Yamaguchi *et al.*, 2018; Fal *et al.*, 2019). Nonetheless, we found that in the enlarged IM and FMs of PcG double mutants, the expression domain of *CLV3* was expanded, while *WUS* expression and domain size were decreased (Fig. 2E–J), indicating uncoupling of stem cell fate and *WUS* expression levels. Our ChIP-Seq data revealed a large number of TFs that gained H3K27me3 during FM determinacy (Fig. 4D), indicating that PcG proteins have a broader function than just silencing of *WUS*. Within the TF genes with increased H3K27me3 levels, we found several HD and MADS genes known to regulate FM determinacy including the floral repressor gene *AGL24* and the pluripotency genes *WUS* and *STM* (Clark *et al.*, 1993; Mayer *et al.*, 1998; Laux *et al.*, 1996; Yu *et al.*, 2004). Although it was suggested that PRC1 directly represses *STM* (Xu and Shen, 2008), *STM* is not an H2Aub target gene, nor does the loss of PRC1 activity result in depletion of H3K27me3 at the *STM* locus (Xu and Shen, 2008; Bratzel *et al.*, 2010; Zhou *et al.*, 2017). In contrast, we showed that the *STM* locus accumulated high H3K27me3 levels during early flower development that were reduced in *emf2-10 vrn2-1* double mutants (Supplementary Fig. S8), while *STM* expression in FMs was temporally extended and maintained beyond flower stage 6 (Fig. 6A–D). This suggests that PRC2-mediated H3K27me3 accumulation is the key silencing mechanism for *STM* during FM determinacy.

Since loss of either *WUS* or *STM* is sufficient for premature FM arrest, it appears redundant to silence both of these and other TF genes that are implicated in promoting meristem activity such as *AGL24*. Nevertheless, our genetic analysis demonstrates that PcG proteins acts through *AGL24*, *STM*, and *WUS* in floral determinacy (Figs 5H, 6E–J). Some hypotheses about the necessity to silence so many TF genes can be drawn from the features of the floral gene regulatory network. (i) Proper flower development also requires silencing of genes well before FM determinacy during flower stage 6, such as *TFL1* at the onset of flower morphogenesis, and *AGL24* after floral stage 2, since the repression of *AGL24* is essential for the activation of the BCE-type MADS box genes to avoid homeotic transformations. (ii) On the other hand, due to the many positive and negative feedback loops in the gene regulatory network, simultaneous silencing of pluripotency genes might be required to avoid compensatory loops such as we described for *WUS* (Müller *et al.*, 2006). The uncoupling of stem cell fate and *WUS* expression levels, which we described here for *emf2-10 vrn2-1* mutant flowers, might be a result of a different compensatory loop. (iii) Both *wus* and *stm* single mutants display limited organogenesis such as their seedlings producing 1–3 leaves before meristem arrest and flowers bearing a number of floral organs. This indicates a certain delay in stem cell termination. Furthermore, *WUS* and *STM*, but also other pluripotency genes such as *PNY* and *PNF*, maintain FMs and the floral stem cell pool through distinct mechanisms (Endrizzi *et al.*, 1996; Ung *et al.*, 2011). Therefore, we propose that synchronized silencing of several pluripotency genes can accelerate FM determinacy in a way that cannot be achieved by silencing *WUS* alone.

Supplementary data

The following supplementary data are available at *JXB* online.

Fig. S1. Test of the internal control *eIF4A* by *TIP41*, *RTFbox*, and *UBQ10* (RT–qPCR).

Fig. S2. Pleiotropic phenotype of *iCLF* flowers.

Fig. S3. Increased size of the vegetative SAM, IM and FMs in *emf2-10 vrn2-1* (*ev*) mutants.

Fig. S4. Enhancement of the valveless phenotype in *clv3-2 emf2-10 vrn2-1* triple mutants.

Fig. S5. *clv/crn emf2-10 vrn2-1* (*ev*) triple mutant flowers.

Fig. S6. Validation of *35S::AP1-GR ap1-1 cal-1* samples before H3K27me3 ChIP-Seq comparing undifferentiated IM tissue (t0) and differentiated flower tissue, 5 d after induction (t5, floral stage 7).

Fig. S7. ChIP-Seq cluster analysis (DiffBind).

Fig. S8. Changes of expression and H3K27me3 levels at MADS box and homeobox genes during early flower development–ChIP-Seq and qPCR validation data.

Fig. S9. H3K27me3 levels of the *AG–WUS* feedback loop.

Fig. S10. Venn diagram comparing H3K27me3 ChIP-seq data (t5) and gene expression (t5) (Ryan *et al.*, 2015).

Fig. S11. Venn diagram comparing published target genes of key floral TFs and H3K27me3 targets.

Fig. S12. ChIP-qPCR of H3K27me3 level at TF genes in *emf2-10 vrn2-1* (*ev*).

Fig. S13. Expression the 12 HD and nine MADS TF genes, which gained H3K27me3 and decreased in expression during early flower development, in *emf2-10 vrn2-1* (*ev*) inflorescence tips using RT–qPCR.

Fig. S14. *LFY* misexpression in *emf2-10 vrn2-1* (*ev*).

Fig. S15. Genetic interaction of strong PcG deficiency and loss of A-function during flower development.

Fig. S16. Loss of H3K27me3 at the *AGL24* locus in *emf2-10 vrn2-1* (*ev*) inflorescences.

Fig. S17. Expression of *AGL24* and *STM* in *clf-28 swn-7* callus-like tissue and *iCLF* inflorescences.

Fig. S18. Rescue of the extra floral organ phenotype in *iCLF* by loss of *STM* (*bum1-3* mutants).

Table S1. Primer list for RT–qPCR.

Table S2. Primer list for ChIP-qPCR.

Table S3. Differentially methylated regions (broad peaks) identified by DiffBind with the DESeq2 method (*P*-value <0.05).

Table S4. Differentially methylated genes (DMGs) identified by ChIPseeker.

Table S5. List of coding genes with increasing H3K27me3 and decreasing expression levels during early flower development.

Table S6. List of coding genes with decreasing H3K27me3 and increasing expression levels during early flower development.

Table S7. miRNA genes changing H3K27me3 levels during early flower development.

Table S8. Genes that are H3K27me3 targets in IM (t0) and/or flowers (t5, floral stage 7).

Table S9. Carpel number and fifth whorl per silique in PcG and *STM*-deficient flowers (percent).

Acknowledgements

Seeds were kindly provided by Frank Wellmer, Yuling Jiao, and Wolfgang Werr. We thank Marc Somssich for critical reading and comments on the manuscript, and Rüdiger Simon for sharing plasmids for RNA *in situ* hybridization. The authors would like to thank the HPC Service of ZEDAT, Freie Universität Berlin, for computing time.

Author contributions

All authors performed the experiments; RMX and JG: design; RMX and QX: writing with the help of RA and JT; LV and GW: performing the bioinformatics analysis with the technical support of SoC and SuC.

Conflict of interest

The authors declare that they have no conflicts of interest.

Funding

This work was kindly funded by the National Natural Science Foundation of China (project nos 31640054 and 31771602), the Fundamental Research Funds for the Central Universities (project no. 2572020DY06), and the Northeast Forestry University Starting Grant for Distinguished Young Scholars.

Data availability

The ChIP-Seq data were deposited in the Gene Expression Omnibus under the series GSE159988. All other relevant data are available within the paper and its supplementary data published online.

References

Alvarez-Buylla ER, Benítez M, Corvera-Poiré A, *et al*. 2010. Flower development. The Arabidopsis Book **8**, e0127.

Baroux C, Gagliardini V, Page DR, Grossniklaus U. 2006. Dynamic regulatory interactions of Polycomb group genes: MEDEA autoregulation is required for imprinted gene expression in Arabidopsis. Genes & Development **20**, 1081–1086.

Bennett L, Melchers B, Proppe B. 2020. CURTA. A general-purpose high-performance computer. ZEDAT, Freie Universität Berlin.

Blázquez MA, Soowal LN, Lee I, Weigel D. 1997. LEAFY expression and flower initiation in Arabidopsis. Development **124**, 3835–3844.

Bradley D, Ratcliffe O, Vincent C, Carpenter R, Coen E. 1997. Inflorescence commitment and architecture in Arabidopsis. Science **275**, 80–83.

Brand U, Fletcher JC, Hobe M, Meyerowitz EM, Simon R. 2000. Dependence of stem cell fate in Arabidopsis on a feedback loop regulated by CLV3 activity. Science **289**, 617–619.

Bratzel F, López-Torrejón G, Koch M, Del Pozo JC, Calonje M. 2010. Keeping cell identity in Arabidopsis requires PRC1 RING-finger homologs that catalyze H2A monoubiquitination. Current Biology **20**, 1853–1859.

Causier B, Schwarz-Sommer Z, Davies B. 2010. Floral organ identity. 20 years of ABCs. Seminars in Cell & Developmental Biology **21**, 73–79.

Chanvivattana Y, Bishopp A, Schubert D, Stock C, Moon Y-H, Sung ZR, Goodrich J. 2004. Interaction of Polycomb-group proteins controlling flowering in Arabidopsis. Development **131**, 5263–5276.

Chu T, Xie H, Xu Y, Ma R. 2010. Regulation pattern of the FRUITFULL (FUL) gene of *Arabidopsis thaliana*. Chinese Journal of Biotechnology **26**, 1546–1554.

Clark, SE, Running M, PMeyerowitz, EM. 1993. CLAVATA1, a regulator of meristem and flower development in Arabidopsis. Development **119**, 397–418.

Clark SE, Running MP, Meyerowitz EM. 1995. CLAVATA3 is a specific regulator of shoot and floral meristem development affecting the same processes as CLAVATA1. Development **121**, 2057–2067.

Coen ES, Meyerowitz EM. 1991. The war of the whorls. Genetic interactions controlling flower development. Nature **353**, 31–37.

Daum G, Medzihradszky A, Suzaki T, Lohmann JU. 2014. A mechanistic framework for noncell autonomous stem cell induction in Arabidopsis. Proceedings of the National Academy of Sciences, USA **111**, 14619–14624.

Diévart A, Dalal M, Tax FE, Lacey AD, Huttly A, Li J, Clark SE. 2003. CLAVATA1 dominant-negative alleles reveal functional overlap between multiple receptor kinases that regulate meristem and organ development. The Plant Cell **15**, 1198–1211.

Ditta G, Pinyopich A, Robles P, Pelaz S, Yanofsky MF. 2004. The SEP4 gene of *Arabidopsis thaliana* functions in floral organ and meristem identity. Current Biology **14**, 1935–1940.

Endrizzi K, Moussian B, Haecker A, Levin JZ, Laux T. 1996. The SHOOT MERISTEMLESS gene is required for maintenance of undifferentiated cells in Arabidopsis shoot and floral meristems and acts at a different regulatory level than the meristem genes WUSCHEL and ZWILLE. The Plant Journal **10**, 967–979.

Engelhorn J, Blanvillain R, Kröner C, Parrinello H, Rohmer M, Posé D, Ott F, Schmid M, Carles C. 2017. Dynamics of H3K4me3 chromatin

marks prevails over H3K27me3 for gene regulation during flower morphogenesis in *Arabidopsis thaliana*. Epigenomes **1**, 8.

Fal K, Cortes M, Liu M, Collaudin S, Das P, Hamant O, Trehin C. 2019. Paf1c defects challenge the robustness of flower meristem termination in *Arabidopsis thaliana*. Development **146**, 17337 7.

Fletcher JC, Brand U, Running MP, Simon R, Meyerowitz EM. 1999. Signaling of cell fate decisions by CLAVATA3 in Arabidopsis shoot meristems. Science **283**, 1911–1914.

Gaspar JM. 2018. Improved peak-calling with MACS2. bioRxiv. doi: https://doi.org/10.1101/496521. [Preprint].

Goslin K, Zheng B, Serrano-Mislata A, *et al*. 2017. Transcription factor interplay between LEAFY and APETALA1/CAULIFLOWER during floral initiation. Plant Physiology **174**, 1097–1109.

Grandi V, Gregis V, Kater MM. 2012. Uncovering genetic and molecular interactions among floral meristem identity genes in *Arabidopsis thaliana*. The Plant Journal **69**, 881–893.

Gregis V, Sessa A, Colombo L, Kater MM. 2006. AGL24, SHORT VEGETATIVE PHASE, and APETALA1 redundantly control AGAMOUS during early stages of flower development in Arabidopsis. The Plant Cell **18**, 1373–1382.

Gregis V, Sessa A, Colombo L, Kater MM. 2008. AGAMOUS-LIKE24 and SHORT VEGETATIVE PHASE determine floral meristem identity in Arabidopsis. The Plant Journal **56**, 891–902.

Gregis V, Sessa A, Dorca-Fornell C, Kater MM. 2009. The Arabidopsis floral meristem identity genes AP1, AGL24 and SVP directly repress class B and C floral homeotic genes. The Plant Journal **60**, 626–637.

Gross-Hardt R, Lenhard M, Laux T. 2002. WUSCHEL signaling functions in interregional communication during Arabidopsis ovule development. Genes & Development **16**, 1129–1138.

Hartmann U, Höhmann S, Nettesheim K, Wisman E, Saedler H, Huijser P. 2000. Molecular cloning of SVP. A negative regulator of the floral transition in Arabidopsis. The Plant Journal **21**, 351–360.

Huang Z, Shi T, Zheng B, Yumul RE, Liu X, You C, Gao Z, Xiao L, Chen X. 2017. APETALA2 antagonizes the transcriptional activity of AGAMOUS in regulating floral stem cells in *Arabidopsis thaliana*. New Phytologist **215**, 1197–1209.

Hugouvieux V, Silva CS, Jourdain A, Stigliani A, Charras Q, Conn V, Conn SJ, Carles CC, Parcy F, Zubieta C. 2018. Tetramerization of MADS family transcription factors SEPALLATA3 and AGAMOUS is required for floral meristem determinacy in Arabidopsis. Nucleic Acids Research **46**, 4966–4977.

Immink RGH, Tonaco IAN, de Folter S, Shchennikova A, van Dijk ADJ, Busscher-Lange J, Borst JW, Angenent GC. 2009. SEPALLATA3: the 'glue' for MADS box transcription factor complex formation. Genome Biology **10**, R24.

Irish VF, Sussex IM. 1990. Function of the apetala1 gene during Arabidopsis floral development. The Plant Cell **2**, 741–753.

Ji L, Liu X, Yan J, *et al*. 2011. ARGONAUTE10 and ARGONAUTE1 regulate the termination of floral stem cells through two microRNAs in Arabidopsis. PLoS Genetics **7**, e1001358.

Jing T, Ardiansyah R, Xu Q, Xing Q, Müller-Xing R. 2020. Reprogramming of cell fate during root regeneration by transcriptional and epigenetic networks. Frontiers in Plant Science **11**, 613.

Kaufmann K, Wellmer F, Muiño JM, *et al*. 2010. Orchestration of floral initiation by APETALA1. Science **328**, 85–89.

Kayes JM, Clark SE. 1998. CLAVATA2, a regulator of meristem and organ development in Arabidopsis. Development **125**, 3843–3851.

Kempin SA, Savidge B, Yanofsky MF. 1995. Molecular basis of the cauliflower phenotype in Arabidopsis. Science **267**, 522–525.

Kirch T, Simon R, Grünewald M, Werr W. 2003. The DORNRÖSCHEN/ENHANCER OF SHOOT REGENERATION1 gene of Arabidopsis acts in the control of meristem cell fate and lateral organ development. The Plant Cell **15**, 694–705.

Krizek BA, Bantle AT, Heflin JM, Han H, Freese NH, Loraine AE, Melzer R. 2021. AINTEGUMENTA and AINTEGUMENTA-LIKE6 directly regulate floral homeotic, growth, and vascular development genes in young Arabidopsis flowers. Journal of Experimental Botany **72**, 5478–5493.

Lafos M, Kroll P, Hohenstatt ML, Thorpe FL, Clarenz O, Schubert D. 2011. Dynamic regulation of H3K27 trimethylation during Arabidopsis differentiation. PLoS Genetics **7**, e1002040.

Laux T, Mayer KF, Berger J, Jürgens G. 1996. The WUSCHEL gene is required for shoot and floral meristem integrity in Arabidopsis. Development **122**, 87–96.

Lenhard M, Bohnert A, Jürgens G, Laux T. 2001. Termination of stem cell maintenance in Arabidopsis floral meristems by interactions between WUSCHEL and AGAMOUS. Cell **105**, 805–814.

Li X, Zheng Y, Xing Q, *et al*. 2020. Ectopic expression of the transcription factor CUC2 restricts growth by cell cycle inhibition in Arabidopsis leaves. Plant Signaling & Behavior **15**, 1706024.

Liao Y, Smyth GK, Shi W. 2014. featureCounts: an efficient general purpose program for assigning sequence reads to genomic features. Bioinformatics **30**, 923–930.

Liljegren SJ, Gustafson-Brown C, Pinyopich A, Ditta GS, Yanofsky MF. 1999. Interactions among APETALA1, LEAFY, and TERMINAL FLOWER1 specify meristem fate. The Plant Cell **11**, 1007–1018.

Liu C, Teo ZWN, Bi Y, Song S, Xi W, Yang X, Yin Z, Yu H. 2013. A conserved genetic pathway determines inflorescence architecture in Arabidopsis and rice. Developmental Cell **24**, 612–622.

Liu C, Xi W, Shen L, Tan C, Yu H. 2009. Regulation of floral patterning by flowering time genes. Developmental Cell **16**, 711–722.

Liu C, Zhou J, Bracha-Drori K, Yalovsky S, Ito T, Yu H. 2007. Specification of Arabidopsis floral meristem identity by repression of flowering time genes. Development **134**, 1901–1910.

Liu L, Farrona S, Klemme S, Turck FK. 2014. Post-fertilization expression of FLOWERING LOCUS T suppresses reproductive reversion. Frontiers in Plant Science **5**, 164.

Liu X, Kim YJ, Müller R, Yumul RE, Liu C, Pan Y, Cao X, Goodrich J, Chen X. 2011. AGAMOUS terminates floral stem cell maintenance in Arabidopsis by directly repressing WUSCHEL through recruitment of Polycomb Group proteins. The Plant Cell **23**, 3654–3670.

Liu X, Dinh TT, Li D, Shi B, Li Y, Cao X, Guo L, Pan Y, Jiao Y, Chen X. 2014. AUXIN RESPONSE FACTOR 3 integrates the functions of AGAMOUS and APETALA2 in floral meristem determinacy. The Plant Journal **80**, 629–641.

Lohmann JU, Hong RL, Hobe M, Busch MA, Parcy F, Simon R, Weigel D. 2001. A molecular link between stem cell regulation and floral patterning in Arabidopsis. Cell **105**, 793–803.

Lopez-Vernaza M, Yang S, Müller R, Thorpe F, Leau E. de, Goodrich J. 2012. Antagonistic roles of SEPALLATA3, FT and FLC genes as targets of the polycomb group gene CURLY LEAF. PLoS One **7**, e30715.

Mayer KF, Schoof H, Haecker A, Lenhard M, Jürgens G, Laux T. 1998. Role of WUSCHEL in regulating stem cell fate in the Arabidopsis shoot meristem. Cell **95**, 805–815.

Melzer R, Verelst W, Theissen G. 2009. The class E floral homeotic protein SEPALLATA3 is sufficient to loop DNA in 'floral quartet'-like complexes in vitro. Nucleic Acids Research **37**, 144–157.

Michaels SD, Ditta G, Gustafson-Brown C, Pelaz S, Yanofsky M, Amasino RM. 2003. AGL24 acts as a promoter of flowering in Arabidopsis and is positively regulated by vernalization. The Plant Journal **33**, 867–874.

Ming F, Ma H. 2009. A terminator of floral stem cells. Genes & Development **23**, 1705–1708.

Moyroud E, Minguet EG, Ott F, *et al*. 2011. Prediction of regulatory interactions from genome sequences using a biophysical model for the Arabidopsis LEAFY transcription factor. The Plant Cell **23**, 1293–1306.

Mozgova I, Hennig L. 2015. The polycomb group protein regulatory network. Annual Review of Plant Biology **66**, 269–296.

Müller R, Borghi L, Kwiatkowska D, Laufs P, Simon R. 2006. Dynamic and compensatory responses of Arabidopsis shoot and floral meristems to CLV3 signaling. The Plant Cell **18**, 1188–1198.

Müller R, Bleckmann A, Simon R. 2008. The receptor kinase CORYNE of Arabidopsis transmits the stem cell-limiting signal CLAVATA3 independently of CLAVATA1. The Plant Cell **20**, 934–946.

Müller-Xing R, Clarenz O, Pokorny L, Goodrich J, Schubert D. 2014. Polycomb-group proteins and FLOWERING LOCUS T maintain commitment to flowering in *Arabidopsis thaliana*. The Plant Cell **26**, 2457–2471.

Müller-Xing R, Schubert D, Goodrich J. 2015. Non-inductive conditions expose the cryptic bract of flower phytomeres in *Arabidopsis thaliana*. Plant Signaling & Behavior **10**, e1010868.

Nägeli C. 1858. Ueber das Wachsthum des Stammes und der Wurzel bei den Gefässpflanzen. In: Beiträge zur Wissenschaftlichen Botanik. Leipzig: Wilhelm Engelmann; 1–11.

Pelaz S, Ditta GS, Baumann E, Wisman E, Yanofsky MF. 2000. B and C floral organ identity functions require SEPALLATA MADS-box genes. Nature **405**, 200–203.

Pelaz S, Gustafson-Brown C, Kohalmi SE, Crosby WL, Yanofsky MF. 2001. APETALA1 and SEPALLATA3 interact to promote flower development. The Plant Journal **26**, 385–394.

Ratcliffe OJ, Bradley DJ, Coen ES. 1999. Separation of shoot and floral identity in Arabidopsis. Development **126**, 1109–1120.

Ryan PT, Ó'Maoiléidigh DS, Drost H-G, Kwaśniewska K, Gabel A, Grosse I, Graciet E, Quint M, Wellmer F. 2015. Patterns of gene expression during Arabidopsis flower development from the time of initiation to maturation. BMC Genomics **16**, 488.

Schoof H, Lenhard M, Haecker A, Mayer KFX, Jürgens G, Laux T. 2000. The stem cell population of Arabidopsis shoot meristems is maintained by a regulatory loop between the CLAVATA and WUSCHEL genes. Cell **100**, 635–644.

Schubert D, Clarenz O, Goodrich J. 2005. Epigenetic control of plant development by Polycomb-group proteins. Current Opinion in Plant Biology **8**, 553–561.

Schuettengruber B, Bourbon H-M, Di Croce L, Cavalli G. 2017. Genome regulation by Polycomb and Trithorax: 70 years and counting. Cell **171**, 34–57.

Scofield S, Murray JAH. 2006. KNOX gene function in plant stem cell niches. Plant Molecular Biology **60**, 929–946.

Serrano-Mislata A, Goslin K, Zheng B, Rae L, Wellmer F, Graciet E, Madueño F. 2017. Regulatory interplay between LEAFY, APETALA1/CAULIFLOWER and TERMINAL FLOWER1: new insights into an old relationship. Plant Signaling & Behavior **12**, e1370164.

Shivram H, Le SV, Iyer VR. 2019. PRC2 activates interferon-stimulated genes indirectly by repressing miRNAs in glioblastoma. PLoS One **14**, e0222435.

Smyth DR, Bowman JL, Meyerowitz EM. 1990. Early flower development in Arabidopsis. The Plant Cell **2**, 755–767.

Somssich M, Je BI, Simon R, Jackson D. 2016. CLAVATA–WUSCHEL signaling in the shoot meristem. Development **143**, 3238–3248.

Soyars CL, James SR, Nimchuk ZL. 2016. Ready, aim, shoot: stem cell regulation of the shoot apical meristem. Current Opinion in Plant Biology **29**, 163–168.

Spillane C, MacDougall C, Stock C, Köhler C, Vielle-Calzada JP, Nunes SM, Grossniklaus U, Goodrich J. 2000. Interaction of the Arabidopsis polycomb group proteins FIE and MEA mediates their common phenotypes. Current Biology **10**, 1535–1538.

Stark R, Brown G. 2011. DiffBind: differential binding analysis of ChIP-Seq peak data. Cambridge: Cancer Research UK - Cambridge Institute, University of Cambridge.

Su YH, Zhou C, Li YJ, Yu Y, Tang LP, Zhang WJ, Yao WJ, Huang R, Laux T, Zhang XS. 2020. Integration of pluripotency pathways regulates stem cell maintenance in the Arabidopsis shoot meristem. Proceedings of the National Academy of Sciences, USA **117**, 22561–22571.

Sun B, Looi L-S, Guo S, He Z, Gan E-S, Huang J, Xu Y, Wee W-Y, Ito T. 2014. Timing mechanism dependent on cell division is invoked by Polycomb eviction in plant stem cells. Science **343**, 1248559.

Sun B, Xu Y, Ng K-H, Ito T. 2009. A timing mechanism for stem cell maintenance and differentiation in the Arabidopsis floral meristem. Genes & Development **23**, 1791–1804.

Sun B, Zhou Y, Cai J, *et al*. 2019. Integration of transcriptional repression and polycomb-mediated silencing of WUSCHEL in floral meristems. The Plant Cell **31**, 1488–1505.

Sun D, Li Y, Ma Z, Yan X, Li N, Shang B, Hu X, Cui K, Koiwa H, Zhang X. 2021. The epigenetic factor FVE orchestrates cytoplasmic SGS3–DRB4–DCL4 activities to promote transgene silencing in Arabidopsis. Science Advances **7**, abf3898.

Ung N, Lal S, Smith HMS. 2011. The role of PENNYWISE and POUND-FOOLISH in the maintenance of the shoot apical meristem in Arabidopsis. Plant Physiology **156**, 605–614.

Velanis CN, Herzyk P, Jenkins GI. 2016. Regulation of transcription by the Arabidopsis UVR8 photoreceptor involves a specific histone modification. Plant Molecular Biology **92**, 425–443.

Wagner D, Sablowski RW, Meyerowitz EM. 1999. Transcriptional activation of APETALA1 by LEAFY. Science **285**, 582–584.

Wellmer F, Alves-Ferreira M, Dubois A, Riechmann JL, Meyerowitz EM. 2006. Genome-wide analysis of gene expression during early Arabidopsis flower development. PLoS Genetics **2**, e117.

Williams L, Fletcher JC. 2005. Stem cell regulation in the Arabidopsis shoot apical meristem. Current Opinion in Plant Biology **8**, 582–586.

Xiao J, Jin R, Wagner D. 2017. Developmental transitions: integrating environmental cues with hormonal signaling in the chromatin landscape in plants. Genome Biology **18**, a019315.

Xu L, Shen W-H. 2008. Polycomb silencing of KNOX genes confines shoot stem cell niches in Arabidopsis. Current Biology **18**, 1966–1971.

Yadav RK, Perales M, Gruel J, Girke T, Jönsson H, Reddy GV. 2011. WUSCHEL protein movement mediates stem cell homeostasis in the Arabidopsis shoot apex. Genes & Development **25**, 2025–2030.

Yamaguchi N, Huang J, Tatsumi Y, *et al*. 2018. Chromatin-mediated feed-forward auxin biosynthesis in floral meristem determinacy. Nature Communications **9**, 5290.

Yan Z, Shi H, Liu Y, Jing M, Han Y, Wellmer F. 2020. KHZ1 and KHZ2, novel members of the autonomous pathway, repress the splicing efficiency of FLC pre-mRNA in Arabidopsis. Journal of Experimental Botany **71**, 1375–1386.

Yu G, Wang L-G, He Q-Y. 2015. ChIPseeker: an R/Bioconductor package for ChIP peak annotation, comparison and visualization. Bioinformatics **31**, 2382–2383.

Yu H, Ito T, Wellmer F, Meyerowitz EM. 2004. Repression of AGAMOUS-LIKE 24 is a crucial step in promoting flower development. Nature Genetics **36**, 157–161.

Yumul RE, Kim YJ, Liu X, Wang R, Ding J, Xiao L, Chen X. 2013. POWERDRESS and diversified expression of the MIR172 gene family bolster the floral stem cell network. PLoS Genetics **9**, e1003218.

Zhang X, Clarenz O, Cokus S, Bernatavichute YV, Pellegrini M, Goodrich J, Jacobsen SE. 2007. Whole-genome analysis of histone H3 lysine 27 trimethylation in Arabidopsis. PLoS Biology **5**, e129.

Zhao L, Kim Y, Dinh TT, Chen X. 2007. miR172 regulates stem cell fate and defines the inner boundary of APETALA3 and PISTILLATA expression domain in Arabidopsis floral meristems. The Plant Journal **51**, 840–849.

Zhou Y, Romero-Campero FJ, Gómez-Zambrano A, Turck F, Calonje M. 2017. H2A monoubiquitination in *Arabidopsis thaliana* is generally independent of LHP1 and PRC2 activity. Genome Biology **18**, 69.